UNIVERSITY OF JYVÄSKYLÄ
DEPARTMENT OF CHEMISTRY
RESEARCH REPORT No. 130

ULTRAFAST ELECTRON TRANSFER FROM POTENTIAL ORGANIC AND METAL CONTAINING SOLAR CELL SENSITIZERS

BY

PASI MYLLYPERKIÖ

Academic Dissertation
for the Degree of
Doctor of Philosophy

Jyväskylä, Finland
2009

DEPARTMENT OF CHEMISTRY, UNIVERSITY OF JYVÄSKYLÄ
RESEARCH REPORT No. 130

ULTRAFAST ELECTRON TRANSFER FROM POTENTIAL ORGANIC AND METAL CONTAINING SOLAR CELL SENSITIZERS

BY

PASI MYLLYPERKIÖ

Academic Dissertation
for the degree of
Doctor of Philosophy

To be presented, by permission of the Faculty of Mathematics and Science of the University of Jyväskylä, for public examination in Auditorium FYS1, on February 6th 2009, at 12 noon

Jyväskylä, Finland
ISBN 978-951-39-3468-2
ISSN 0357-346X

URN:ISBN:978-952-86-0181-4
ISBN 978-952-86-0181-4 (PDF)
ISSN 0357-346X

University of Jyväskylä, 2024

Abstract

In this Thesis ultrafast spectroscopic techniques were used to study electron transfer processes in dye sensitized nanocrystalline semiconductor films as well as excitation relaxation in metal complexes in solution. The main interest was to clarify the mechanisms of heterogenous electron transfer in $Ru(dcbpy)_2(NCS)_2$ sensitized nanocrystalline TiO_2 films, the active electrode of one of the most promising dye sensitized solar cells. It was established that the 'slow' picosecond injection occurs from a triplet states that could be directly populated by excitation of the red side of the MLCT band of the sensitizer. Heterogeneity of the injection was shown to originate from an inter-ligand electron transfer and to be dependent not only on relative positions of the excited triplet states of the sensitizer and the conduction band edge, but also on the coupling strength between the sensitizer and the semiconductor states. New results were obtained on electron injection from three aminophenyl dyes to nanocrystalline TiO_2 films. All of these dyes showed sub 300 fs electron injection rates. It was found that one of the dyes containing flexible substituents in the terminal amino group underwent an extremely fast excited state isomerization that took place in parallel with the electron transfer, reducing the over all efficiency of injection. For RuN3 sensitizer in solution detailed studies of dynamics were carried out. Finally excited state dynamics of a metal complex $Fe(aceylacetonato)_3$ in solution was studied by using UV excitation and mid-infrared probing. It was observed that after excitation the system underwent electronic relaxation from the initially excited state to a vibrationally hot state from where after cooling the system relaxed back to the ground state. Some evidence was obtained for mode selective transfer of vibronic excess energy to the solvent bath.

A substantial effort was put in to build experimental setups and data collection and analysis programs. Several designs utilizing non-linear optical amplifiers; one stage and two stage versions for visible spectral region as well as an optical parametric amplifier for mid-infrared region were realized. Data acquisition and data analysis software packages were developed for a number of measuring schemes. These included a user friendly interface to control and record data from pump and probe experiments either by reading individual photodiodes or diode arrays at 1 kHz repetition rate of the laser. Data analysis packages included software for fitting of kinetic traces and global analysis software.

Author's address
Pasi Myllyperkiö
Department of Chemistry
P.O. Box 35
FI-40014 University of Jyväskylä
Finland
pasi.m.myllyperkio@jyu.fi

Supervisor
Professor Jouko Korppi-Tommola
Department of Chemistry
P.O. Box 35
FI-40014 University of Jyväskylä
Finland

Reviewers
Professor Leif Hammarström
Department of Photochemistry & Molecular Science
Uppsala University
Uppsala, Sweden

Professor Josef Wachtveitl
Institute of Physical and Theoretical Chemistry
Johann Wolfgang Goethe-University Frankfurt
Frankfurt/Main, Germany

Opponent
Professor Guglielmo Lanzani
Diparmento di Fisica, ULTRAS-INFM
Politechnico di Milano
Milano, Italy

Preface

The present work has been carried out at the Department of Chemistry, University of Jyväskylä. Part of the research was done jointly with the Department of Chemical Physics, Lund University. The last experiments were done in Politecnico di Milano in collaboration with Professor Giulio Cerullo.

I am very grateful to my supervisor Professor Jouko Korppi-Tommola for introducing me to the world of femtosecond spectroscopy and photo-induced electron transfer reactions and for finding the funding for the years. You offered a great opportunity to find my own interests on the field and in trying and building new things in the lab. Special thanks belong to Professor Villy Sundström and Dr. Arkady Yartsev for giving great opportunity to work with you in very enthusiastic and scientific atmosphere in Lund. With you I learned a lot about the science, especially your way of working with positive attitude and that there is always time for the results. I would like to thank Professors Mika Pettersson and Henrik Kunttu for the present projects with femtosecond mid-IR spectroscopy.

Thank you all past and present collogues at the Department of Chemisrty in Jyväskylä and in Chemical Physics in Lund, together we have had so many unforgettable moments. Especially I would like to thank Jani Kallioinen and Viivi Lehtovuori for the years we were learning and working together, and traveling around the world. Special thanks to Heikki Häkkänen for great friendship over the years, it was so nice to "kuukkeloida", and have many scientific and non-scientific discussions. I wish also thank office and technical personnel in Jyväskylä, especially Eki, Tapsa and Jussi, for all help during the years; so many times I have been asking different things for the lab. From Lund especially thanks to Gabor, Mathias, Donatas, Yuri, Tonu and Wichard for both scientific and free time activities we had.

I want to thank from all my hart my parents Pekka and Marja from the all the kind gratuitous support I have got during the years, my brothers Petri and Ilkka and their families for the interest towards this Thesis, now it is finally done. I also wish to thank all friends, and especially "the ghetto posse", for all nice activities we have had.

The financial support from Academy of Finland, Graduate School for Energy Science and Technology funded by the Ministry of Education of Finland for a scholarship are gratefully acknowledged, as well as support from LASERLAB-EUROPE large scale facility program.

Jyväskylä, November 2008
Pasi Myllyperkiö

Original publications

This thesis is a review based on the following original research papers, which will be referred to in the text by their Roman numerals.

I **Transient absorption studies of the $Ru(dcbpy)_2(NCS)_2$ excited state and the dye cation on nanocrystalline TiO_2 film**,
J. Kallioinen, V. Lehtovuori, P. Myllyperkiö, J. Korppi-Tommola,
Chem. Phys. Lett. **2001** 340, 217-221.

https://doi.org/10.1016/S0009-2614(01)00398-0

II **Photoinduced electron injection from $Ru(dcbpy)_2(NCS)_2$ to SnO_2 and TiO_2 nanocrystalline films**,
G. Benkö, P. Myllyperkiö, J. Pan, A.P. Yartsev, V. Sundström,
J. Am. Chem. Soc. **2003**, 125, 1118-1119.

https://doi.org/10.1021/ja029025j

III **Interligand electron transfer determines triplet excited state electron injection in RuN3-sensitized TiO_2 films**,
G. Benkö, J. Kallioinen, P. Myllyperkiö, F. Trif, J. Korppi-Tommola, A.P. Yartsev, V. Sundström,
J. Phys. Chem. B **2004**, 108, 2862-2867.

https://doi.org/10.1021/jp036778z

IV **A Study of Electron Transfer in $Ru(dcbpy)_2(NCS)_2$ Sensitized Nanocrystalline TiO_2 and SnO_2 Films Induced by Red Wing Excitation**,
P. Myllyperkiö, G. Benkö, J. Korppi-Tommola, A.P. Yartsev, V. Sundström,
Phys. Chem. Chem. Phys., **2008**, 10, 966-1002.

https://doi.org/10.1039/B713515G

V **PhotoInduced interfacial electron injection in RuN3-TiO_2 thin films: Resolving picosecond timescale injection from the triplet state of the protonated and deprotonated dyes**,
M. Pellnor, P. Myllyperkiö, J. Korppi-Tommola, A.P. Yartsev, V. Sundström,
Chem. Phys. Lett., **2008**, 462, 205-208.

https://doi.org/10.1016/j.cplett.2008.07.066

VI **Photo-Induced Electron Transfer from Series of Acrylic Acid Dye Sensitizers to Titanium Dioxide Nanoparticles**,
P. Myllyperkiö, C. Manzoni, D. Polli, G. Cerullo, J. Korppi-Tommola,
J. Phys. Chem. C, Submitted **2008**.

https://doi.org/10.1021/jp902226y

VII **Ultrafast Electronic and Vibrational Energy Relaxation of $Fe(acetylacetonate)_3$ in Solution**.
E.M.S. Macoas, R. Kananavicius, P. Myllyperkiö, M. Pettersson, H. Kunttu,
Journal of Physical Chemistry A **2007**, 111, 2054-2061.

https://doi.org/10.1021/jp066271z

Some selected publications related to the field of the Thesis, but are not included in the Thesis:

1. **Energy transfer in LH2 of Rhodospirillum molischianum, studied by subpicosecond spectroscopy and configuration interaction exciton calculations**,
J.A. Ihalainen, J. Linnanto, I.H.M. van Stokkum, P. Myllyperkiö, B. Ücker, H. Scheer, J.E.I. Korppi-Tommola,
J. Phys. Chem. B **2001**, 105, 9849-9856.

2. **Effects of ligand substitution on the excited state dynamics of the Ru(dcbpy)$(CO)_2$$I_2$ complex**,
V. Lehtovuori, J. Kallioinen, P. Myllyperkiö, M. Haukka, J. Korppi-Tommola,
Chem. Phys. **2003**, 295, 81-88.

3. **Transient midinfrared study of light induced dissociation reaction of Ru(dcbpy)$(CO)_2$$I_2$ in solution**,
V. Lehtovuori, J. Aumanen, P. Myllyperkiö, M. Rini, E.T.J. Nibbering, J. Korppi-Tommola,
J. Phys. Chem. A **2004**, 108, 1644-1649.

4. **Photoinduced ultrafast dynamics of Ru(dcbpy)$_2$$(NCS)_2$-sensitized nanocrystalline TiO_2 films: the influence of sample preparation and experimental conditions**,
J. Kallioinen, G. Benkö, P. Myllyperkiö, L. Khriachtchev, B. Skårman, R. Wallenberg, M. Tuomikoski, J. Korppi-Tommola, V. Sundström, A. Yartsev,
J. Phys. Chem. B **2004**, 108, 6365-6373.

5. **Study of mechanisms of light-induced dissociation of Ru(dcbpy)$(CO)_2$$I_2$ in solution down to 20 fs time resolution**,
V. Lehtovuori, P. Myllyperkiö, J. Linnanto, C. Manzoni, D. Polli, G. Cerullo, J. Korppi-Tommola,
J. Phys. Chem. B **2005**, 109, 17538-17544.

6. **Time-resolved coherent anti-Stokes Raman-scattering measurements of I_2 in solid Kr: Vibrational dephasing on the ground electronic state at 2.6-32K**,
T. Kiviniemi, J. Aumanen, P. Myllyperkiö, M. Pettersson,
J. Chem. Phys. **2005**, 123, 06-4509.

7. **Relaxation Dynamics of Cr$(acac)_3$ Probed by Ultrafast Infrared Spectroscopy**,
E.M.S. Maçôas, R. Kananavicius, P. Myllyperkiö, M. Pettersson, H. Kunttu,
J. Am. Chem. Soc. **2007**, 129, 8934-8935.

Abbreviations

DAS	decay assosiated spectra
DSSC	dye sensitised solar cell
EM	electromagnetic
ESA	excited state absorption
ET	electron transfer
GS	ground state
HOMO	highest occupied molecular orbital
IR	infrared
ISC	intersystem crossing
LMCT	ligand-to-metal charge transfer
LUMO	lowest unoccupied molecular orbital
MC	metal centered
MIR	mid-IR
MLCT	metal-to-ligand charge transfer
NOPA	non-collinear Optical Parametric Amplifier
PV	photovoltaic
UV	ultraviolet
vis	visible

Contents

Chapter 1

Introduction

Life on earth would not be possible in the darkness. The Sun provides us a huge amount of light energy every day, 15000 times more than we consume, and this energy will not run out in a very near future. Nature has evolved to use the flow of photons from Sun efficiently via photosynthesis, the driving force of life. Photosynthesis is still a mystery for us. Intensive study of the extremely complicated molecular processes that allow fixing carbon dioxide from air and splitting water from soil to produce oxygen and carbohydrates powered by energy from photons has been going on for more than 100 years. Yet photosynthesis serves us as a model to develop much more simple devices, molecular solar cells that can produce electricity from Sun's photons even at much higher efficiency than photosynthesis converts light energy into chemical energy. Increasing demand for and the limited stock of fossil fuels has triggered growing interest to develop artificial devices that could covert light energy directly into electricity or into hydrogen by splitting water. In general, photoactive systems where light energy is converted into chemical energy are in the interest of a broad field of the researchers. For the future, it is a great challenge and an opportunity to find and develop new methods that utilize Sun's energy and convert it into usable forms. Sunlight is the power source for the photovoltaic (PV) cells. Today nearly 12000 MW of PV power has been installed for use in everyday life[1]. Majority of PV capacity is based on silicon technology, and annual growth rates of this business sector have exceeded 30% during several past years.

New, the third generation[2] solar cells that are based on molecular light

[1]Source: Worldwatch; Prometheus Institute; REN21.

[2]The first generation solar cells, typically single crystalline silicon devices, suffer high manufacturing and installation costs. The second generation devices typically consisting of polycrystalline $CuInGaSe_2$ or Si semiconductor thin films were significantly cheaper, but their efficiency needs to be enhanced in order to make them practically viable[1].

harvesting have been developed[1]. Two major developments are on the way, both having promise to cheap low temperature roll-to-roll manufacturing. One of them is based on organic materials imbedded in a polymer forming a two-phase blend of p- and n-type semiconductors that have a very large surface area[2]. So far these devices have shown efficiencies at best exceeding 5%[3] and roll-to-roll manufacture has been demonstrated. The second development is based on dye sensitized nanocrystalline titanium dioxide active electrode, so called Grätzel Cell or dye sensitized solar cell (DSSC), and an electrolyte solution (liquid or solid) to carry over the charge from the catalyst covered counter electrode[4]. DSSC's have shown 11% conversion efficiency on glass substrate and 5% efficiency on plastic substrate[5]. Since such devices are still in the development stage several physical processes that make them work are not thoroughly understood. For example in the Grätzel cell there are several processes the details of which are not fully understood e.g. electron injection mechanism from organic or metal based sensitizers, electron diffusion through the nanocrystalline TiO_2 electrode, the nature of the recombination reactions, details of the catalytic process on the counter electrode etc. Understanding these details is necessary for systematic development of the cell efficiency.

In this thesis study of electron transfer from the photo-excited dye molecules to nanocrystalline semiconductor films has been the central theme, but also desire to understand other possible relaxation channels in the microscopic molecular world has been a motivation for this work. Mature optical spectroscopic methods have proven to be efficient in the study of these processes. In optical spectroscopy EM-radiation in the frequency region from 10^{16} to 10^{12} Hz (wavelength from 50 nm to 100 μm) is used to convey information of the properties of the molecular system (energy levels, identities and structures) under study by absorption, emission or scattering of electromagnetic radiation (see figure 1.1). The development of light sources, especially lasers that can provide extremely short light pulses over a wide range of frequencies, has brought the time dimension into optical spectroscopy. Today real time information about molecular level processes can be recorded routinely by using ultrafast laser spectroscopy, offering a possibility to study small details of light induced molecular processes, processes that finally are the underlying reason to changes in macroscopic devices that we can see with a naked eye.

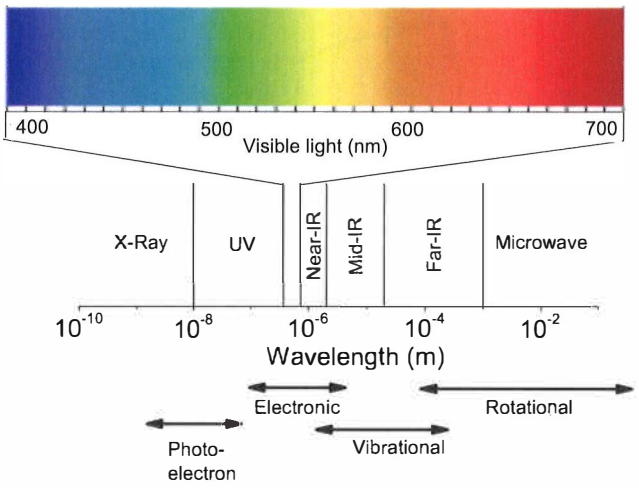

Figure 1.1: Regions of the electromagnetic spectrum.

1.1 Dye-sensitized solar cell

Dye-sensitized solar cell[4, 6] has shown potential to become a cost efficient power source for low-power devices. It has been demonstrated that the cell can be manufactured on plastic substrates, using low temperatures under normal conditions. Low processing temperature means lower energy consumption during manufacturing process. Many different semiconductor materials have been investigated as active electrode materials, mainly metal oxide and metal sulphide semiconductors [7–9]. Metal based sensitizers have shown up to 11% efficiency on glass substrate and the record efficiency for organic sensitizers is 8%[10]. On plastic substrates the efficiency has remained at 5% level, so far. Major improvement in DSSC compared to early designs at 70's was to replace a flat surface with nanostructured semiconductor particles, which increased the effective active surface drastically[6].

1.1.1 Sensitization of wide-bandgap semiconductors

The idea of spectral sensitization of wide band-gap semiconductor by organic molecules is from the 60's[11, 12]. Even some earlier studies of sensitization of ZnO powder by adsorbed Rhodamine B, Eosin, Erythrosin and cyanine dyes exists [13]. Ruthenium polypyridyl complexes were used for the first time as sensitizers on SnO_2 in the 70's by Gleria and Memming[13, 14].

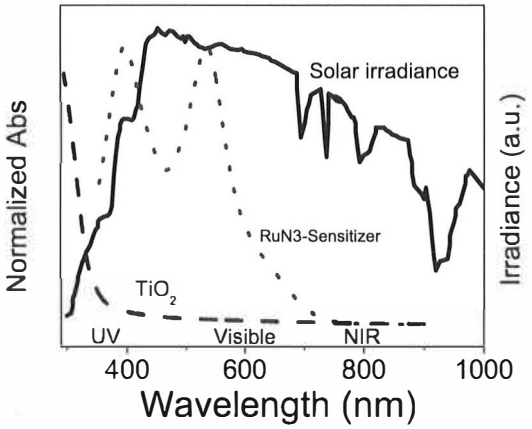

Figure 1.2: Effect of sensitization on the spectrum of a wide band-gap semiconductor (dashed) induced by a light absorbing dye (dotted). Solar spectrum (solid) is shown for reference.

Without sensitization the wide band-gap semiconductor film absorbs only the UV part of solar radiation, but after attachment of the dye absorption covers main part of the visible radiation of the solar spectrum (see figure 1.2). Sensitizer molecule is anchored via covalent binding onto the surface of a nanocrystalline semiconductor material (see figure 1.3). Anchoring occurs normally from solution phase spontaneously via the following chemical groups; carboxy- (-O-(C=O)-), phosphate- (-O-(HPO2)-), silanyl- (-O-Si-) or amide group (-NH-(C=O)-)[7, 15–17]. Since the dye is covalently bound to the semiconductor surface there is a coupling between electronic states of the dye and the conduction band states for electron transfer to occur with high efficiency[18]. Typical sensitizers are metal complexes or organic dyes having large extinction coefficients in the visible or near-IR regions[16, 19–26].

Sensitization may be used for both n-type and p-type semiconductors. In n-type sensitization dye injects electrons to the conduction band of the semiconductor, and this is the most common approach to make dye-sensitized solar cells[6]. In a p-type sensitization, photogenerated holes are injected from the sensitizer in the valence band of the semiconductor[27–30]. This requires different properties from the semiconductors, for n-type sensitization conduction band states and lowest empty electronic orbitals of the sensitizer molecule have to be on same level while highest occupied orbitals is on bandgap region. For p-type sensitization situation is opposite, valence

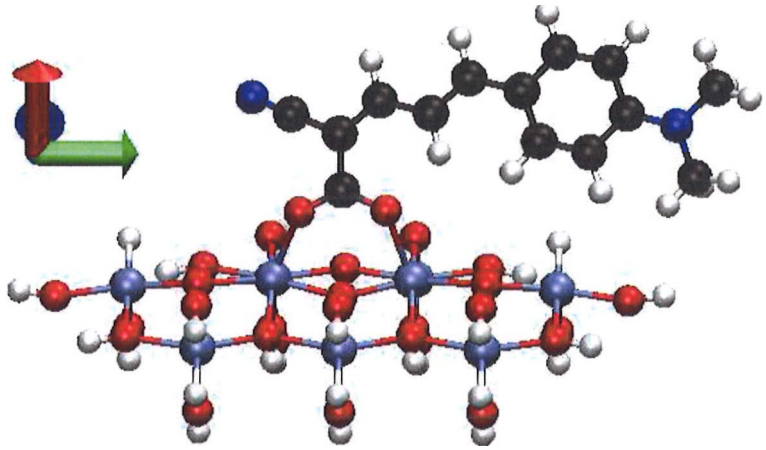

Figure 1.3: Dye attachment via an anchoring carboxylic-group.

band states have to remain on same level as HOMO orbitals of the sensitizer and LUMOs on bandgap region. See figure 1.4. Second difference is that in n-type process dye cation is formed while in p-type injection anion is formed.

Metal complexes that have been found to be good sensitizers are strong absorbers in the visible region, efficient electron injectors and photochemically stable. In such complexes the central metal has often d^3 or d^6 electron configuration and low oxidation number (for ruthenium 2+) and ligands with a low-lying π-electron system[31]. It is also suggested that molecules having small reorganization between ground state and oxidation geometries are more stable for continuous redox cycle[7].

Efforts to improve light absorption efficiency of the dye-sensitized solar cells have increased interest in organic dye sensitizers. Conjugated organic dyes offer several advantages over metal complex dyes: 1) potential for cheap production 2) large absorption coefficient in the visible spectral region 3) molecular design allows tuning of the redox potentials and improving the absorption coefficients[10]. The major disadvantage of the organic sensitizers is their relatively narrow spectral absorption band width in the visible region and their weak resistance against photodegradation. However, high absorption coefficient combined with relatively narrow absorption band width opens possibilities to prepare specific light absorbers or colorful devices by just changing the sensitizer molecule. So far coumarins have been found to

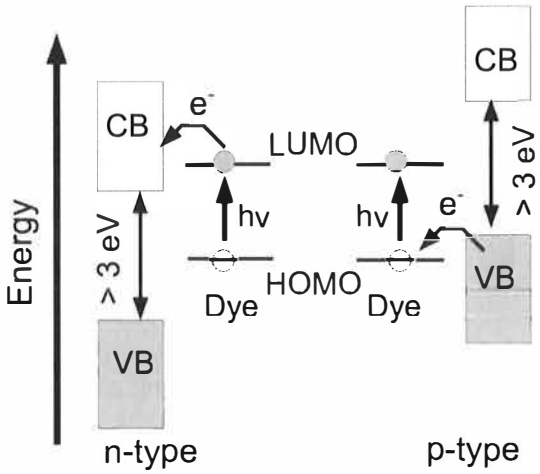

Figure 1.4: Sensitization of n- and p-type semiconductors. HOMO highest occupied molecular orbital, LUMO lowestest unoccupied molecular orbital, VB valence band CB conduction band.

be most efficient and promising organic sensitizer molecules[10].

1.1.2 Structure and operation of DSSC

The dye-sensitized solar cell is actually a photoelectrochemical cell that is driven with photon energy. Schematic presentation of the structure and the fundamental processes of the DSSC are presented in figure 1.5. First functional steps in the cell are the absorption of a photon followed by oxidation of the dye due to electron injection to the semiconductor. These processes are followed by a subsequent electron transport through network of semiconductor nanoparticles to the conducting layer of the active electrode from where electrons are taken to the external load. The electrolyte receives the electrons from the external circuit via the counter electrode. A redox I^-/I_3^- pair completes the current cycle where the final stage is the delivery of the electron from I^- to the dye cation.

Electron injection efficiency is dependent of the relative positions of the excited state of the sensitizer and the conduction band edge and the density of states of the semiconductor and the coupling between the two. It has been found that the electrolyte solvent has an effect on forward injection rate, the most commonly used solvent acetonitrile giving the fastest rates[32]. In addition adsorption of the electrolyte cations (e.g. Li^+ or TBA^+) in the functioning cell results in reduction of the conduction band edge of the semiconductor, lowering depending on the cation[33, 34]. Since in the present Thesis only sensitized films in pure solvents (acetonitrile and 3-metoxypropionitrile) were studied effects of electrolyte ion adsorption on forward injection could not be addressed. For RuN3 sensitizer it was assumed that in the solvents used the degree of protonation of the dye is negligible as well as proton adsorption on the semiconductor surface.

1.2 Femtochemistry and ultrafast spectroscopy

Femtochemistry, more than twenty years old research field now, may be defined as a field of research that focuses on the study of physical, chemical and biological events in real time by making use of very short optical pulses[35]. During this short time period it has grown to be important and well established field of research, where previously unexpected new dimensions have been developed recently, multidimensional optical spectroscopy (analogous to multidimensional NMR spectroscopy)[36–38], attosecond spectroscopy[39, 40], time resolved electron diffraction[41] and X-ray spectroscopy[42–45]. In 1999 Nobel Price in Chemistry was awarded to Pro-

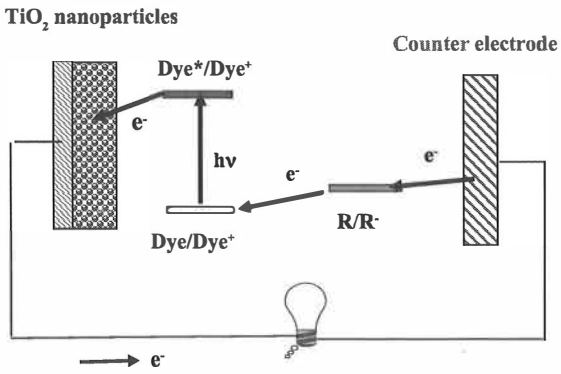

Figure 1.5: Electron cycle in the DSSC.

fessor Ahmed H. Zewail, who has been involved widely in the development of different areas of the femtochemistry, as they are today.

Nowadays ultrashort laser pulses can be produced from X-ray to THz spectral regions, almost continuously. Availability of such pulses has been one of the main reasons for a fast development of the field and applications. During last ten years development of the non-collinear parametric amplification of white light seed pulses has made it possible to produce sub-10 fs laser pulses in the visible and near IR region[46–50]. Non-linear optical parametric amplifiers (NOPA) have become reliable and easy to use light sources for time resolved spectroscopy with sub 30-fs resolution in everyday laboratory work [51, 52]. Such time resolution allows real time observation of the coherent nuclear oscillations and gives detailed information about electron-vibration interactions in molecular systems[53]. Simultaneously general understanding of quantum mechanics of the molecular excited states and light matter interactions has opened new insights to understand spectroscopic results from linear and non-linear responses, our kaleidoscope into the molecular world.

In ultrafast pump-probe spectroscopy a fs-laser pulse is used to excite the system coherently. A very large number of molecules experience the excitation in the excitation volume simultaneously and start evolving in time along a characteristic reaction or relaxation coordinates of the system. This evolution can be monitored in multiple ways, but in all methods the parameter that monitors the time behavior of the system is the time delay between the excitation and the detection. Common method in femtosecond spectroscopy is to use one fs-pulse for triggering the photo physical event and to probe induced changes in time by a delayed second pulse. A number of simultaneous processes may occur in molecules after pulsed excitation in

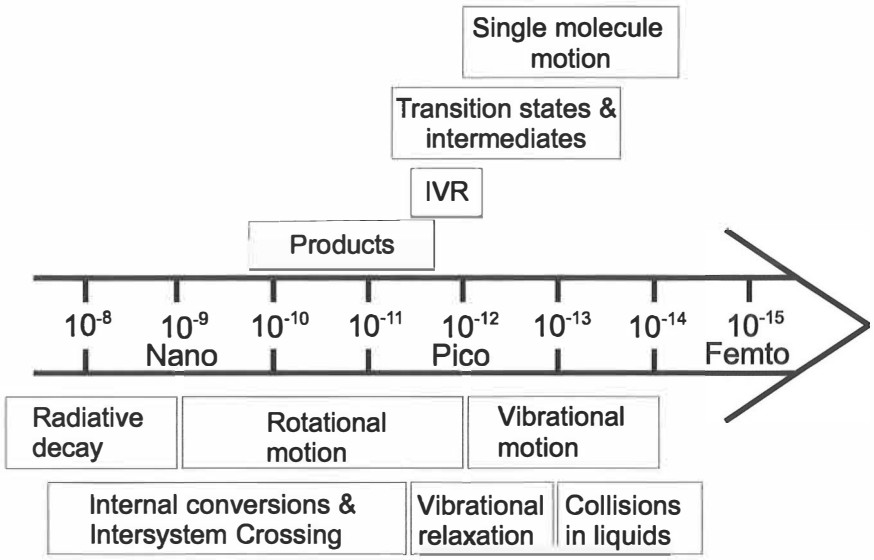

Figure 1.6: Time scales for different processes. Adapted from Zewail's article[35]

sub nanosecond time scale (see figure 1.6). In photochemical reactions electron distribution is induced by light. The speed of electrons sets an upper limit to the rate of any chemical process. It has been claimed that such time domain is in order of 0.1 fs, 10^{-16}s[54], meaning that all photochemical and photo-physical processes are slower than this upper limit. However, transitions between two levels are limited by zero point motion of nuclei, and that sets the upper limit for the transitions to be in order of 10^{-14} seconds[31, 54]. Chemical reactions such as dissociation or addition reactions or non-reactive photo events, such as structural changes, light emission, charge transfer, internal conversion, intersystem crossing etc. may proceed after excitation with a short laser pulse. Here in we will focus on processes that are initiated in the electronic excited state(s) of molecules populated after absorption of photons of a very short light pulse. In Chapter 2 further discussion on detection scheme, optical arrangements and data collection are presented.

1.3 Excited state dynamics

Typically electronic excitation of a molecule occurs by absorption of visible or ultra violet (UV) photon. The energy of the incident photon should be in res-

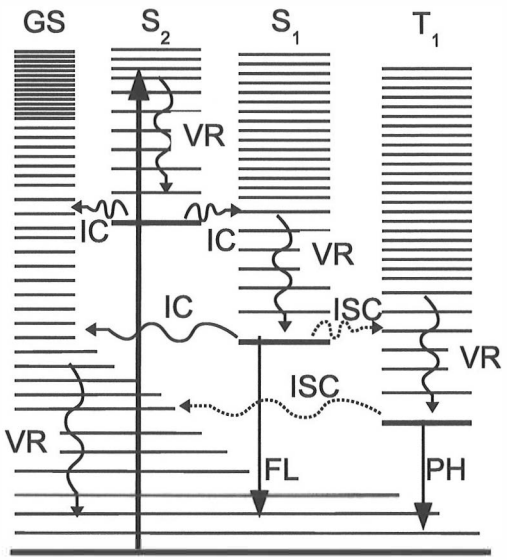

Figure 1.7: Jablonski diagram showing different relaxation channels for photoexcited molecule. (VR=vibrational relaxation, IC=internal conversion, ISC=intersystem crossing, FL=fluorescence and PH=phosphorence.

onance with electronic transition to be excited, i.e. energy difference between corresponding vibronic states should be approximately the same as that of the incident photon. Excitation promotes both electronic and vibrational energy to the molecule and excited state begins to evolve in time. Evolution of excited state may lead to vibronic relaxation back to ground state and photochemical reactions. Vibronic relaxation can lead to other electronic states and redistribution or dissipation of the excess vibrational energy. As shown in figure 1.6 each process has its own time domain, and reaction rates depend on the molecule and its surroundings. Photochemical reactions form new molecular species through excited states, e.g. isomerization, electron transfer or addition/dissociation reactions. Vibrational relaxation and isomerization may occur in the electronic ground state as well. In figure 1.7 are presented different relaxation channels for the initially excited S_2 state, the lowest energy singlet excited state S_1, the lowest energy triplet state T_1 and the ground electronic state GS (or S_0). For metal complexes having tens of atoms, there are typically many close lying states that offer complicated relaxation channels and have an impact on the observed lifetimes[31, 55].

Electronic states and transitions in metal complexes are named by using terminology from Ligand Field theory. Shortly, if electronic transitions take

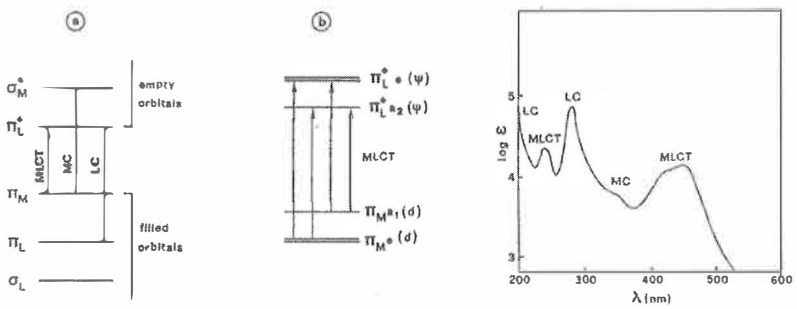

Figure 1.8: Schematic presentation of lowest energy electronic transitions in a metal complex $Ru(bpy)_3^{2+}$ and the corresponding absorption spectrum[56].

place from metal orbitals to ligand orbitals it is called metal-to-ligand charge transfer and state the transition is called metal-to-ligand charge transfer (MLCT) transition and the state metal-to-ligand charge transfer state. Other commonly used nomenclature includes ligand centered (LC), metal centered (MC) and ligand-to-metal charge transfer (LMCT) transitions (See Figure 1.8)[13, 56, 57].

1.3.1 Vibrational cooling

Electronic excitation deposits a large amount of excess energy to vibrational modes in the excited electronic states. Redistribution and removal of excess energy can be separated to two, intramolecular and intermolecular, processes. In the intramolecular process non-thermal energy distribution of vibrational excess energy is distributed over vibrational modes via internal vibrational energy redistribution (IVR), while intermolecular processes are responsible for transferring energy to the bath surrounding the solute, solution, crystal lattice or protein vibrational and translational energy through collisions[58–62]. Vibrational energy redistribution usually leads to statistical distribution of the populations over vibrational modes, and can be characterized by vibrational temperature at that specific electronic state[61, 62]. IVR-Rate constant depends on the size of the system, i.e. number of vibrational modes and density of vibrational states, and couplings between these states[58]. Large variety of IVR rates have been reported in the literature, varying from <1 ps to tens (or even hundreds) of picoseconds[58, 61–63].

Intermolecular vibrational energy transfer may occur simultaneously or subsequently to internal vibrational energy redistribution. Vibrational

temperature of a statistically thermalized state may be higher than that of environment, and when the system relaxes into vibrational equilibrium with its environment, excess vibrational energy is transferred to surroundings through anharmonic coupling to low frequency modes, via collisions or phonons[60]. Typically vibrational cooling occurs at rates in the order of $10^{11}s^{-1}$-$10^{12}s^{-1}$[59, 64–66].

1.3.2 Internal conversion, intersystem crossing and radiative relaxation

Initially formed electronic excited state may relax to lower electronic states via internal conversion (IC) or intersystem crossing (ISC). These processes are non-radiative and mediated by molecular vibrations. If the density of electronic states is high, conversion to other electronic states may occur much faster than vibrational relaxation, even in sub picosecond timescale[57]. Conversion to state having same multiplicity is called IC and state with different spin multiplicity ISC, respectively. In metal complexes high density of states together with strong spin-orbit coupling may mediate ultrafast (<100 fs) intersystem crossing[31, 67 69]. Population of an excited triplet state may decay through a cascade type mechanism with parallel internal conversion and ISC competing with each other[70].

Both radiative and non-radiative processes may relax the initially prepared population of the excited electronic state to the ground state. In latter process electronic energy is transferred to vibrational modes of the electronic ground state[71, 72]. Vibrational energy redistribution and relaxation in the electronic excited and ground states in real time have also been studied extensively by using ultrafast techniques.[65, 73–75]. In the radiative process excess electronic energy is released by emission of a photon, and no heat is generated.

1.3.3 Solvent relaxation

Solvent reorganization after electronic excitation of a solute is called excited state solvation relaxation. This process is due to sudden increase in the dipole moment of the solute in its ground state solvent environment due to excitation. After excitation the solute and the solvent shell have to adjust to a new equilibrium and the energy of the excited state will be lowered. Typically solvation occurs in the time scale from picoseconds to hundreds of picoseconds, and is strongly dependent on dielectric properties of the solvent[57, 59, 76].

1.3.4 Excited state lifetimes

Above excited state deactivation channels were shortly described. The lifetime of the excited state (τ) is dependent of the sum of the rates of all possible deactivation processes. In the simplest case, typically the lowest excited state, only radiative and non-radiative channels are functional, giving total lifetime for the state

$$\frac{1}{\tau} = k_r + k_{nr}, \tag{1.1}$$

where k_r and k_{nr} are the rate constants for the radiative and non-radiative processes. Non-radiative processes may be temperature dependent (Arrhenius type processes), while radiative lifetime remains constant[65, 69]. In addition to the described deactivation processes, excited state reactions may occur after excitation. Several such reactions have been identified, e.g. intermolecular light induced charge transfer[19, 31, 57, 77, 78], elimination, dissociation and substitution reactions[31, 35, 57, 79–81] or structural changes[35, 37, 82–84]. Ultrafast spectroscopy has been widely used to study such photophysical phenomena.

1.3.5 Interfacial electron transfer

Interfacial electron transfer is an important fundamental phenomenon that drives catalytic processes and is the first step in many photochemical surface reactions. Electron transfer in such systems have been studied intensively during the last century[19, 77]. In the development of the theory of electron transfer reactions on solid/liquid interface, Marcus has had a important role [85–88]. However, other researchers and research groups have given also seminal contribution to the development and understanding of interfacial electron transfer reactions, like Gerischer, Levich, Dogodnaze and Sakata. See references [89–91]. Broad interest to electron transfer on the dye-semiconductor interface has risen during past fifteen years because of intensified research and development of dye-sensitized solar cells (DSSC)[4, 6]. During these years basically two types of sensitizer molecules, organic and metal containing complexes, have been tested as light harvesters and electron injection sources in the cell. A large number of sensitizers have been used as probes to study the dynamics of forward electron transfer on the nanoparticle semiconductor interface.

Electron transfer rates from molecular sensitizer to the nanocrystalline semiconductor have been reported to vary from a few femtoseconds to picoseconds depending on the system under study[24, 26, 68, 92–94]. Multiple reasons for such diversity may be seen: energetics, number of ac-

ceptor states, strength of electron transfer couplings, binding geometries and aggregation. Normally ultrafast electron injection is found for the systems where there is strong coupling between absorbing electronic states and the conduction band states of the semiconductor [24, 95]. Metal diimine-complexes have been widely used as sensitizers, and especially electron injection from Ru(2,2'-bipyridine-4,4'-dicarboxylato)$_2$(NCS)$_2$ has been studied intensively because of its exceptionally good performance in the functional DSSC [17, 68, 92, 93, 96–99].

Classically photoinduced electron transfer can be described by a transfer from a photoexcited state to an acceptor state. Electron transfer rate between the two molecular electronic levels can be expressed by using the transition-state theory:

$$k_{et} = k_e \nu_{eff} e^{-E^*/k_b T} \tag{1.2}$$

where k_e is electronic transmission factor obtained from Landau-Zener coefficient [85] (more details can be found also from ref. [100] and references therein), and ν_{eff} is effective frequency along reaction coordinate. The exponential factor depends on the free energy difference and total reorganization energy. In case of weak electronic coupling between donor and acceptor states (i.e. nonadiabatic limit) equation reduces to familiar Fermi's golden rule

$$k_{et} = (2\pi/\hbar)V^2(FC) \tag{1.3}$$

where FC is Frank-Condon weighted density of states. Term depends on the properties of the system and temperature, and is formulated under high-temperature approximation in the following manner [85, 87, 91].

$$FC = \frac{1}{(4\pi\lambda kT)^{\frac{1}{2}}} \exp\{-\frac{(\Delta G^o + \lambda)^2}{4\lambda kT}\} \tag{1.4}$$

In case of strong coupling electron transmission factor becomes unity and if activation barrier is lowered by coupling (E<<kT), the reaction rate becomes directly related to effective frequency, which in some cases is the solvation correlation time[101, 102].

Formulation shows that important rate determining parameters are the change of Gibb's free energy and reorientation energy λ. Electron transfer rate from molecular electronic state to a conduction band of a semiconductor containing multiple electronic states (continuum) can be obtained by summing up all possible two level rates, or in other words by integrating over the energy band. The quantity V in equation 1.3 represents electronic coupling between electron donor and acceptor states. It is notable that as the number of states increases the importance of V vanishes[103]. The initial charge separation between the dye and the semiconductor has been focus of intensive

studies during last ten years and there are still open questions about why electron transfer is so efficient, how fast it finally needs to be for optimal performance of the cell and why it almost in all cases has been shown to be heterogeneous.

1.4 Spectroscopy of Excited states dynamics and photo-product formation

There are different methods to study time-dependent behavior of excited states. All of them have their advantages and disadvantages. Time-resolved emission techniques (e.g. fluorescence up-conversion, time correlated single photon counting and fluorescence streak camera etc.) are efficient tools to study radiative processes and lifetimes. They are spectrally selective method and in many cases monitor only the excited state of interest, but they are limited in giving information about quenching processes or the states above emitting state. The radiative decay constant of spontaneous emission can be measured experimentally by determining spontaneous emission quantum yield and lifetime of the excited state. Transient absorption spectroscopy is a widely used method to study excited state properties and light induced reactions in real time. The advantage of this method is that transient spectra contain information not only on the excited states but also information on possible photo-products. Figure 1.9 shows a schematic presentation of potential energy curves of an electronic ground state and two lowest electronic excited states as a function of a hypothetical reaction coordinate. Arrows in the figure represent possible contributions of the various processes in the transient absorption signal. It is easily seen from figure 1.10 that one of the biggest problems of this technique is that signals (bleach, excited state or product absorptions and stimulated emission) may overlap spectrally, making analysis complicated and often additional information on absorption properties of the transient species are needed for reliable interpretations. The problem is common in the analysis of transient absorption spectra in the visible or in the near infrared regions, i.e. in probing electronic transitions. Effect of vibrational cooling to vibrational spectra is shown in figure 1.11. In systems with a reaction channel often the kinetic fingerprint of the reaction will be observed mixed with several other relaxation processes. Molecular vibrations are directly connected to internal structure of a molecule and spectrally well separated characteristic vibrational bands may be used to monitor the dynamics of interest in the mid-infrared spectral region. For example if in a photochemical reaction a bond is broken,

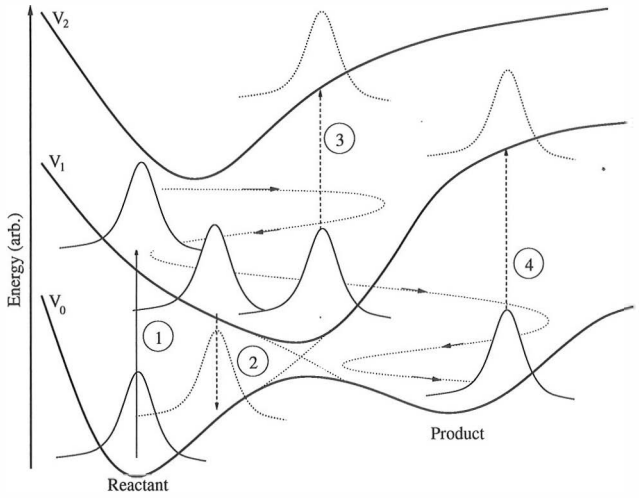

Figure 1.9: Dynamics in the excited states of an arbitrary system. Vertical arrows indicate types of signals that may contribute to transient absorption: 1) photo bleach 2) stimulated emission 3) excited state absorption 4) product absorption.

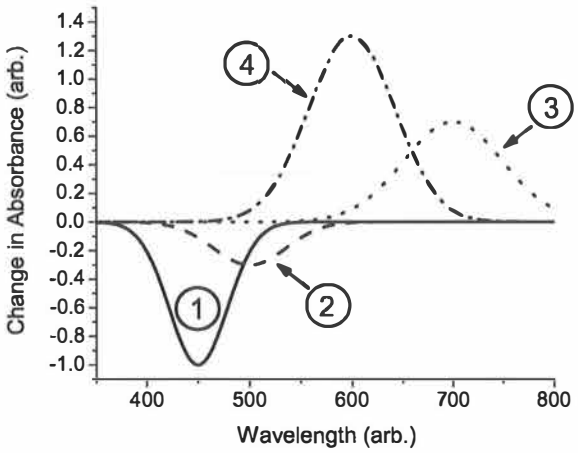

Figure 1.10: Typical spectral signatures of the processes of fig.1.9 in transient absorption experiments. 1) photobleach 2) stimulated emission 3) excited state absorption; 4) product absorption.

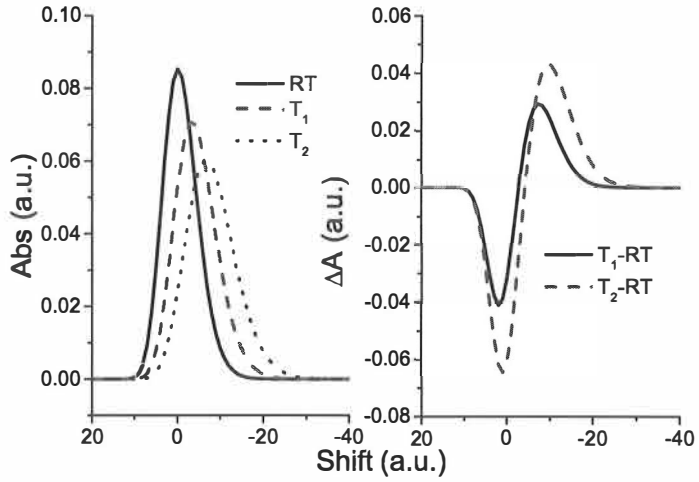

Figure 1.11: Temperature dependent shift in vibrational spectra. Left: Absorption spectra at three different temperatures (T_2>T_1>RT (room temperature)). Right: Differential absorption spectra.

after excitation the corresponding vibrational mode would disappear and a new band characteristic of the photoproduct would emerge in the spectrum giving a clear signature of the occurrence of the reaction. In addition anharmonicity of molecular vibrations means that if the molecule receives excess energy on excitation, high lying vibronic states will be populated and will absorb at red shifted frequencies. By monitoring the time evolution of these red shifted infrared bands information on cooling of the electronically excited molecules will be obtained[65, 75, 104]. Selectivity in the infrared spectral region is much better than in the visible spectral region and dynamic information that is directly related to the molecular structure can be obtained[80]. As an example of a photo-reaction dye cation formation by photo induced electron transfer from a sensitizer dye to the conduction band of a nanocrystalline semiconductor particle is given, a central theme of this thesis. As a simplified case reaction is as follows

$$A + h\nu \longrightarrow A^* \longrightarrow A^+ + e^-(Cond.Band) \tag{1.5}$$

To observe dynamics of such a reaction in the visible spectral region one needs to identify the spectral window where the newly born ionic species absorbs. This has to be made indirectly by creating the cation with some means and

measuring its absorption spectrum separately[105, 106]. If one observes a rise of the transient signal in this particular spectral region one can be fairly confident that emergence of the cation is monitored. Stimulated emission decay for organic sensitizers has been found to be suitable for monitoring electron injection[107]. Electronic absorption from injected electrons in the conduction band of semiconductor has been also used to monitor electron transfer reaction[17, 97, 100, 108, 109].

Chapter 2

Methods

In this chapter experimental details of transient absorption spectroscopy, data collection and data-analysis used in this Thesis will be presented. Examples of the experimental arrangements and data acquisition are mainly taken from the work that has been done in Jyväskylä to build and improve the experimental setups over several years. The purpose of this chapter is to explain the basics of the experiments, what has to be taken care of and how to obtain reliable results from data-analysis, a fact that lies in the hart of ultrafast spectroscopy and never can be overemphasized.

2.1 Transient Absorption Spectroscopy

In Transient absorption spectroscopy temporal evolution of spectral changes of a molecular species induced by a ultrashort laser pulse is recorded. Detection is done by using another short laser pulse for probing absorption changes in the sample and intensity or spectral changes of this second pulse are recorded using photodiodes. If probe pulse is spectrally broad detection wavelength is selected using monochromator or filters, or its done using spectrograph/diode array detection (see figure 2.1).

Spectral changes are often presented as differential absorption signals (either positive (induced absorption) or negative (bleach or stimulated emission), figure 1.10), characteristic of newly created species. Transient spectra or single wavelength kinetic traces are measured by varying timing between excitation and probe pulses. For ultrashort light pulses and small time differences this has to be done by using optical delayline, i.e. traveling distance of one pulse is changed with respect to the other. For a light pulse traveling in air, 1 mm change in path length corresponds to 3.3 ps in time. At a time t=0 both pump and probe pulses are at same time in the sample. At positive de-

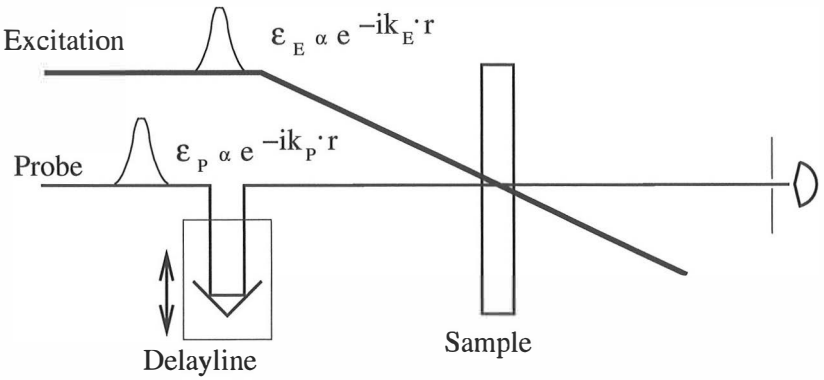

Figure 2.1: Schematic presentation of the non-collinear pump-probe / transient absorption experiment.

lays t+Δt probe pulse passes through the excited volume in the sample after the excitation, and probes changes in the sample absorption/polarization.

Time dependent optical density change at a detection wavelength λ, is defined by the Beer-Lambert law (Eq. 2.1) and is proportional to the population N and absorption coefficient ε of all absorbing states i at time Δt.

$$A[OD](\lambda,\Delta t) = \log \frac{I_0(\lambda)}{I(\lambda,\Delta t)} = \sum_i^n \varepsilon_{i,\lambda} N_i(\Delta t) l \tag{2.1}$$

Often it is much more convenient to present data as a change of absorption compared to ground state absorption. This can be done by using two probe beams one going through the excitation volume ($I\delta t$) and the other just below the excitation volume (I_0) and/or an optical chopper in the excitation beam. To improve signal to noise ratio both options are usually combined, and absorption change is calculated as

$$\Delta A[OD](\lambda,\Delta t) = \log \frac{I_0(\lambda)}{I(\lambda,\Delta t)_{excitation}} - \log \frac{I_0(\lambda)}{I(\lambda,\Delta t)_{no\ excitation}} \tag{2.2}$$

A sample trace is shown in the figure 2.2.

2.1.1 Polarization effects in TA experiments

Absorption of photons in the UV to IR regions is induced by dipole transitions between the initial and the final states. The dipole can be described by a vector having a length and direction, where length is correlated with absorption strength and direction with orientation of the transition moment.

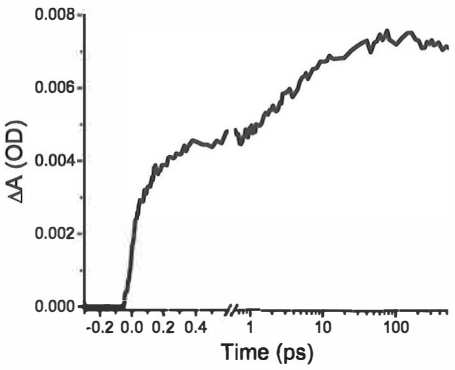

Figure 2.2: Time dependent of excited state absorption change after 535 nm excitation of RuN3 in ethanol, probed by 30 fs pulses with center wavelength of 700 nm (observe the logarithmic scale of the time axis).

In transient absorption experiments information on both quantities may be obtained. In isotropic medium molecules are randomly oriented. A linearly polarized light pulse excites the molecules having their transition dipole moments parallel to the exciting electric field. Pulsed excitation builds a non-uniform orientation distribution of excited molecules in a bath of isotropic distribution of ground state molecules in solution[110]. A 'hole' is created in the ground state population at the time of excitation. The initial (t=0) anisotropies in an isotropic medium for two state transition lie between of 0.4 and -0.20 corresponding to parallel and perpendicular transition dipole orientations with respect to initial absorption dipole orientation, respectively. The created anisotropy may be lost via several mechanisms, by rotational motion, internal conversion between excited states, electron and energy transfer or chemical reactions[110, 111]. Each mechanism has its characteristic time scale and several processes may occur in parallel. A non-exponential anisotropy decay normally is a sign of parallel processes taking place in the sample. In cases where excited state lifetime is long, ground state rotation dominates the dynamics[112]. In transient absorption experiment the probe pulse monitors an excited state population. It is not irrelevant whether you probe the created excited state population with parallel or perpendicular probe pulse, both produce their own decay profiles (see fig. 1.9). Equation 2.1 is valid for both polarizations separately. I_0 is same for both decays since before excitation medium is isotropic, but after excitation both signals have their characteristic time dependencies and absorption coefficients $\varepsilon_{||}$ and $\varepsilon_{\perp}$,

which have been described by Eisenthal [110]. The formulation contains a contribution from the molecules that were not excited and a contribution from the molecules that already have returned to the ground state before arrival of the probe pulse. It has been shown that the probe transmission may contain a contribution from molecule reorientation in the ground and excited states[112]. Ground state has high contribution in the situation where ground state absorption is strong, for example in one-color experiments.

Besides anisotropy measurements transient absorption spectroscopy is used to obtain information on population decays of electronic states. In these experiments the effect of rotational motion has to be eliminated[113]. By recording both time dependent parallel and perpendicular signals separately one can calculate both the anisotropy and the population decay profiles by using Equation 2.3. Population decay may be measured also directly by turning the relative angle between the polarizations of excitation and probe beams to magic angle (MA) of 54.7° with a suitable polarizing element.[113].

$$\mathrm{MA}(t) = \frac{I_{||}(t) + 2I_{\perp}(t)}{3};\ r(t) = \frac{I_{||}(t) - I_{\perp}(t)}{I_{||}(t) + 2I_{\perp}(t)} \tag{2.3}$$

2.2 Experimental setups

In this section experimental setups used in this Thesis will be described in detail. A number of transient absorption setups were used, capable of sub 10 femtosecond time resolution at best. In Jyväskylä two pump-probe setups were developed and their data acquisition systems created during this Thesis work, mostly by the author. The major contribution by the author in the development of the second setup in Jyväskylä was to build several parametric optical amplifiers, two of them double pass NOPA's and one of them a mid-infrared OPA. During research visits to the Chemical Physics group at Lund University two separate femtosecond spectrometers, one with 30 fs time resolution and the other with 130 fs time resolution, were used. In the last paper sub 25 fs UV excitation and sub 10 fs probe setup of the Department of Physics of the Technical University of Milan was deployed.

2.2.1 Light sources and optical parametric amplifiers

A typical fs-spectrometer is based on solid state titanium-sapphire fs-seeder laser and a regenerative amplifier. Output with a central wavelength of about 800 nm is used to pump devices producing tunable femtosecond light pulses. Today the most commonly used tunable femtosecond light sources

are based on optical parametric amplification. In optical parametric amplification initially pump and seed pulses are directed to non-linear crystal. In non-linear crystal pump photons at frequency ω_p generate two coherent photons, the signal ω_s and the idler ω_i, which fulfill the energy conservation relation $\omega_p = \omega_s + \omega_i$. The momentum is conserved as well to fulfill $k_p = k_s + k_i$, which is also called phase-matching condition. As there is a weak seed pulse present in the crystal, it will give a polarization component to a wave at $\omega_p - \omega_s = \omega_i$. If the phase-matching condition is satisfied a wave at ω_i will grow as it travels through the crystal. Simultaneously this new wave at ω_i will beat with ω_p and gives a polarization component to ω_s and adds to the wave at signal frequency. Thus power will be transferred from pump to signal and idler, and initial seed is amplified[114, 115].

Three different OPAs were used in this work based on collinear and non-collinear optical parametric amplification. The main difference between a non-collinear and a collinear amplification is the way how signal and idler pulses propagate through the non-linear crystal. Pulse durations and spectral widths of the amplified pulses depend on the propagation geometry in each case. In collinear amplification there are two important parameters, pulse lengthening and amplification bandwidth. The pulse lengthening originates from differences in group velocities of the idler, the signal and the pump pulses. Since group velocities are not matched for all three waves, it causes the situation where idler travels fastest, and together with pump generates new signal photons at the leading edge of the pulse while new idler photons are generated at the trailing edge of the idler, pulse lengthening can not be avoided. In collinear amplification bandwidth is also limited by the same reason, phase velocities are matched only for certain frequencies at a time. In NOPA configuration the idler propagates into different direction with respect to the signal (See figure 2.3). The angle between pump and seed can be used to match group velocity between signal and idler, in optimum case very broad amplification bandwidth is obtained and no additional pulse lengthening is generated during the amplification process. This mechanism allows for efficient compression of the amplified pulses, which is not possible in collinear amplification[116]. For example pump-seed angle in the non-linear crystal (BBO type I) is around 4 degrees and internal signal angle around 28 degrees, the phase matching bandwidth covers over the visible and near-IR regions[117].

In the visible spectral region NOPA uses a broad band white seed light (extending from 380 nm to 1600 nm) generated in a sapphire plate in combination with the frequency doubled output of the fundamental of the Ti-Sapphire amplifier. Amplification of white light in a BBO (β-barium borate) crystal with the 400 nm pulses results in tunable output from NOPA from

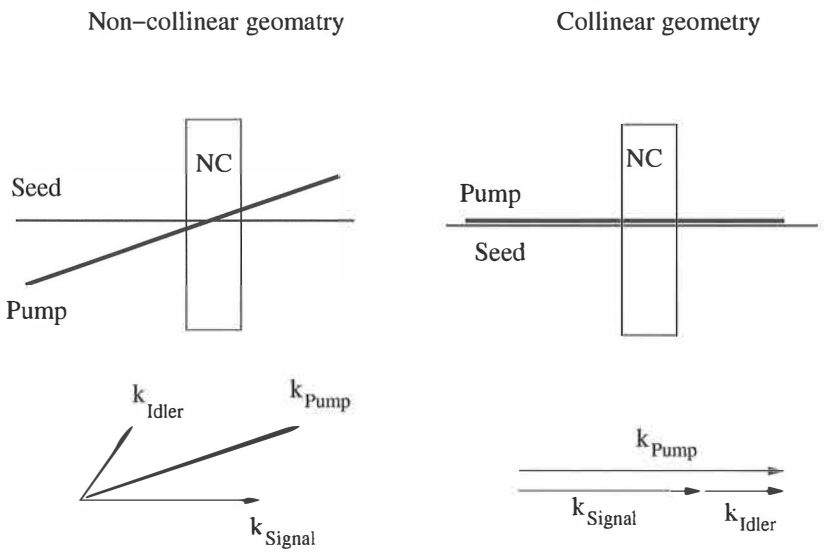

Figure 2.3: Arrangement of the non-collinear and collinear amplification and vector presentations of the corresponding phase matching condition.

470 nm to 750 nm and from 850 nm to 1600 nm with pulse durations of about 30 fs after pulse compression, but even sub-10 fs pulses have been generated[46–50, 118].

The duration of the pulse is limited by its spectral bandwidth. The limitation comes from the Fourier relationship between time and frequency domains. A Gaussian pulse has a Time-Bandwidth Product (TBP) of 0.441. For transform limited pulses a simple relation of

$$\Delta t = \frac{0.441}{c} \frac{\lambda^2}{\Delta\lambda} \tag{2.4}$$

holds, where Δt is the pulse duration is seconds, λ is the central wavelength and $\Delta\lambda$ is the bandwidth (FWHM) in meters and c is the speed of light.

Tunable mid-IR pulses were generated by a two stage optical parametric amplifier in collinear arrangement. The amplifying crystal was a 4-mm BBO which was pumped at 800 nm. Near-IR part of a single filament white light continuum generated in 1-mm thick sapphire plate is used as a seed. The amplifier generates signal radiation (1200-1620 nm; s-polarization) and idler radiation (1520-2500 nm; p-polarization). These two pulses are directed to a 1.5-mm thick $AgGaS_2$ crystal for difference frequency generation to produce femtosecond pulses in the mid-infrared spectral region from 3 to 8 μm [104]. Pulses have typically a spectral bandwidth of 200 cm^{-1} and 100-150

Type (Crystal)	Input 1 (Pump)	Input 2 (Seed)	Output 1 (Signal)	Output 2 (Idler)
OPA (BBO I) (NOPA)	s-pol	p-pol	p-pol	p-pol
OPA (BBO II) (NIR-OPA)	p-pol	s-pol	s-pol	p-pol
SHG (BBO I)	p-pol	p-pol	s-pol	
SFM (BBO I)	p-pol	p-pol	s-pol	
DFM ($AgGaS_2$ II)	s-pol	p-pol	p-pol	

Table 2.1: Polarizations of generated radiation in nonlinear crystals.

fs duration. Pulse energy depends on wavelength and varies from 1 to 4 μJ.

The third optical parametric amplifier used in this work, known with a commercial name 'TOPAS', is a collinear OPA seeded by superfluorescence emitted from a non-linear crystal[119]. The device consists of an independently pumped superfluorescence generator, preamplifiers and a power amplifier. All these stages are geometrically arranged using a single nonlinear crystal. To achieve high reproducibility of generated pulses, all the amplification stages are driven to saturation. With suitable non-linear crystals (Table 2.1) the output can be tuned from 190 nm all the way to 8 μm. The pulse duration is about the same as that of the pump pulse, in best cases 20% shorter.

2.2.2 Transient absorption setup

In the transient absorption experiments of this work in most cases two NOPA's were used to generate the excitation and the probe pulses. In some experiments white light continuum was used for probing as well. In some experiments excitation was extended to the UV spectral region by second harmonic generation of the output from NOPA or by sum frequency mixing the output from NOPA and the fundamental of the laser in a non-linear crystal. In this way it was possible to generate femtosecond excitation pulses from 320 nm to 390 nm and 420 nm to 475 nm, respectively. In figure 2.4 is shown the schematics of the visible transient absorption setup. Excitation and probe pulse intensities were recorded with photodiodes provided with home built preamplifiers. In spectrally resolved transient experiments photodiode arrays were used to record absorption changes induced by the excitation pulse. Additional beam splitter allowed characterization of excitation and probe pulses at the sample position using second order autocorrelation or frequency-resolved optical gating (FROG) technique implemented recently to the setup.

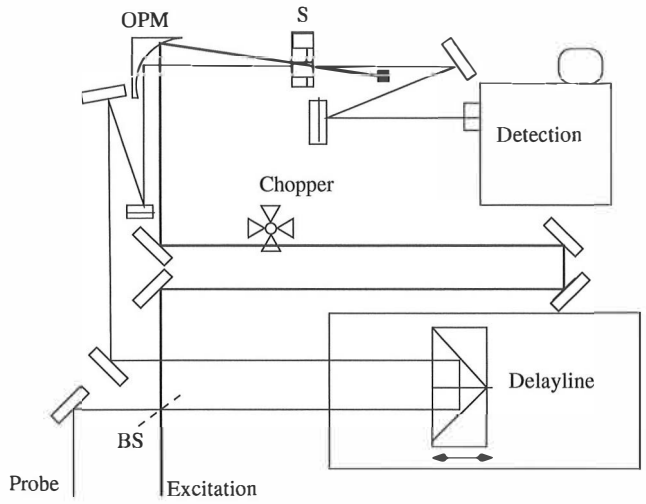

Figure 2.4: Experimental arrangement of visible transient absorption spectrometer. BS=optional beam splitter, OPM=Off-axis parabolic mirror, S=sample/NC crystal.

2.2.3 UV/Vis/mid-IR - mid-IR transient absorption setup in Jyväskylä

The new mid-infrared setup was based on two OPAs, one for generating mid-IR probe pulses, and the TOPAS that was used to generate excitation pulses from UV to mid-IR region (320 nm - 8.0 μm). Detection in the mid-infrared region was based on a 2*64 MCT (HgCdTe) array detector. At the output plane of a 15 cm spectrograph equipped with a grating with 150 grooves/mm a spectral resolution of 1.3 cm^{-1} was obtained within a typical spectral window of 200 cm^{-1} at 5 μm . The system utilizing efficient signal averaging allowed for high sensitivity of detection and measurement of very small absorption changes ($\Delta OD < 10^{-5}$) in the transient infrared spectra.

2.3 Data acquisition

Data collection and processing is in the heart of experimental femtosecond spectroscopy. Interpretation of any time resolved kinetic or spectral results relies on the quality of experimental data and its numerical processing. The author has invested much of his effective research time in developing software suitable for use in the experiments: steering delay lines, reading multiple photodiodes and array detectors (dual MCT (64) and single silicon array

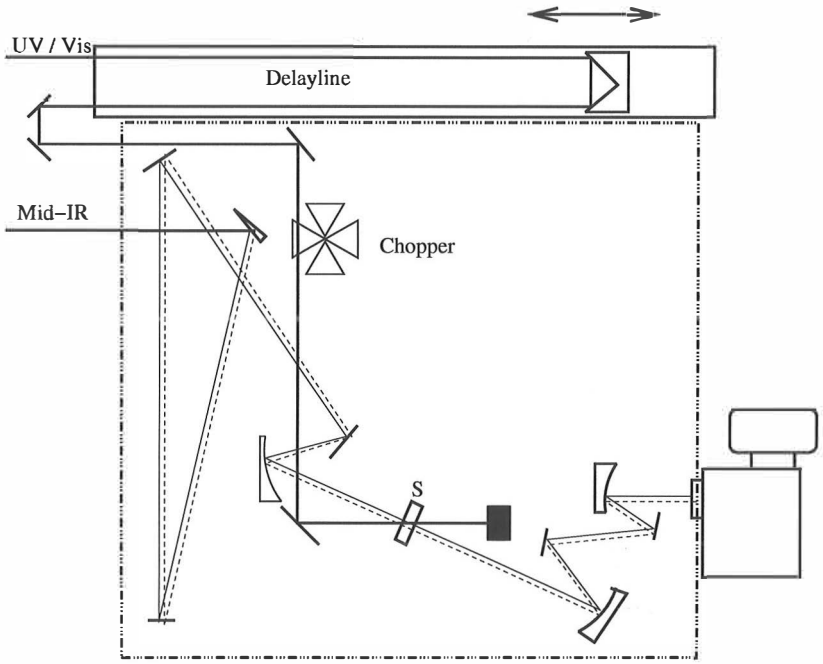

Figure 2.5: Optical layout of the mid-IR transient absorption setup (Paper VII).

(1024)) and making data streams to be stored in the laboratory and office computers in user friendly formats. The PICO developed in the laboratory in the early nineties to serve picosecond experiments has now matured to a massive but user friendly interface to steer and collect data from complicated multipulse femtosecond experiments in the wavelength region from UV to mid-IR. Authors software development has also included codes to help to handle and process ever increasing number streams from the laboratory. One of the many developments has been writing a global analysis program suitable for analysis of multiple wavelength kinetic data based on an assumed kinetic model.

The laboratory data acquisition software allows monitoring data on pulse to pulse basis and by rejecting bad pulses the quality of collected data can be improved considerably. Signal averaging is performed by using two methods, averaging a preset number of pulses at given delay (typically from 500 to 2000) and repeating the delay sweep several times (typically from 5 to 20 times). At each time delay a preset number of pulses or pulse pairs are collected using the software that operates according to the flow scheme presented in figure 2.6. Pulse pair refers to recording the intensities of the probe pulse with and without excitation. For the rejection of the pulses two different methods have been tested. First one is designed for the three photodiode detection system. Rejection is determined by using a preset limit for the intensity of the probe pulse combined with a linearity test between the two probe pulses. In the photodiode array systems rejection criteria is based on intensity and shape testing. The subroutines used are described in more detail in following paragraph.

2.3.1 Calibration and linearity test

Use of two pulse probing improves the S/N-ratio of the measurement. In addition careful adjustment of beam paths and positioning of the photo detectors is needed. The linearity test helps to set boundary conditions for removing bad data points during the measurement. Sudden fluctuations are possible for example due to laser fluctuations or malfunction of the detection electronics (A/D conversion). Two examples of linearity tests are shown in figure 2.7. Figure 2.7 A shows a very good linear correlation between the probe and the reference pulse intensities. In figure 2.7 B a linearity check is shown where the probe beam experiencing excitation was slightly blocked by a mirror mount edge and poor linearity correlation was obtained.

An effect similar to case B will be obtained if the light intensity - voltage response curves of the two detectors are not similar, noise will be increased and sensitivity goes down.

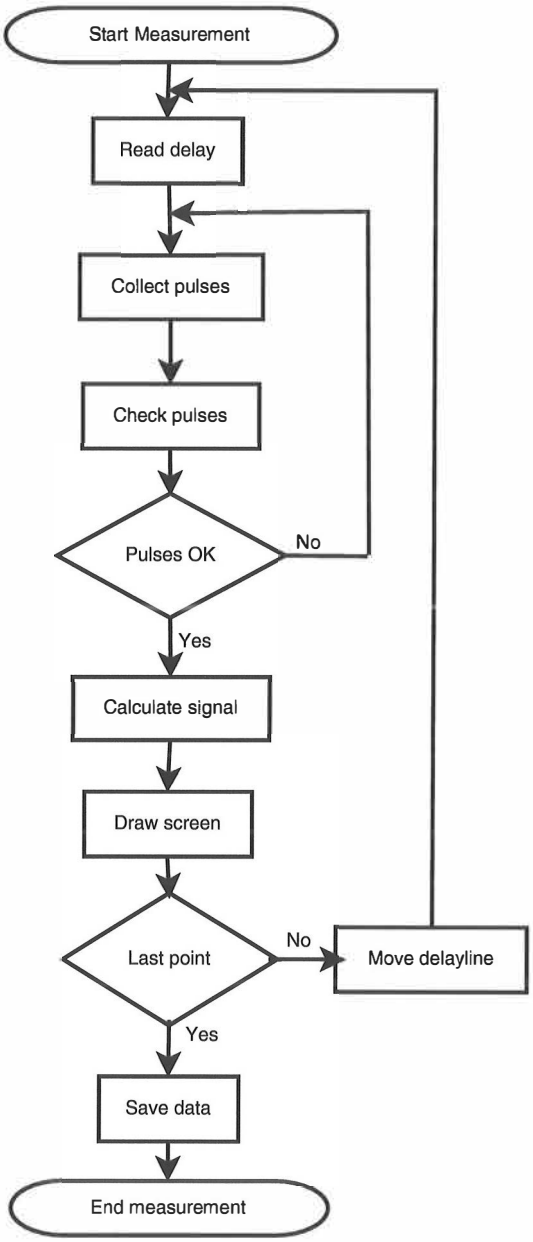

Figure 2.6: General flowchart presentation of the data collection routine in the measurement program.

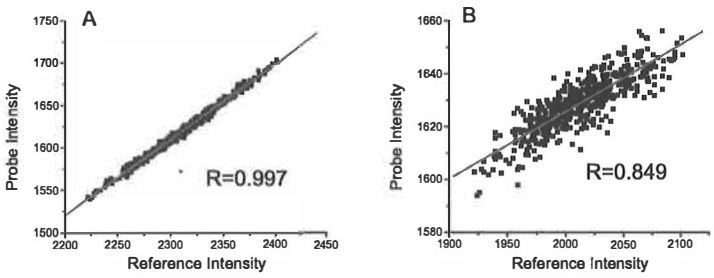

Figure 2.7: Linearity check of probe and reference pulses. A) shows good linearity and B) is an example where the probe beam is partially blocked.

In the beginning of the measurement the user defines the number pulses to be collected at each delay position, stepped at best at 0.7 fs resolution. The intensities of probe and reference pulses are stored into the computer memory. A signal will be accepted or rejected by testing the ratio of the intensities of the pulse pair (or just using intensities). If the ratio falls within the preset limits obtained from the linearity check then the measurement point will be accepted, otherwise rejected. Hence, all pulse pairs are compared individually, and averaging is done after calculation of the absorption change. If the data does not contain the preset number of accepted signals the program will continue measuring additional pulses until the preset averaging condition is met. It is important that number of pulses with and without excitation is in good balance. Final signal, change in absorption at given delay point is stored as an average signal from all accepted pulse pairs. Before averaging program rejects 2.5% of largest and smallest signal values. Change in optical density is calculated according to equation 2.2.

2.4 Instrument response

Characterization of femtosecond pulses used in the experiments is a very important task, autocorrelation functions of the excitation and probe pulses is needed in deconvolution of the recorded kinetic signals to obtain both rise and decay times at best time resolution possible. The traditional and maybe most common methods to record such profiles are second order auto- and cross-correlation techniques. In such measurements intensity profiles rising from second order correlation are recorded. More sophisticated methods are needed to obtain information about relative phases of frequencies within the pulse envelopes. As the spectral bandwidth of a femtosecond pulse increases

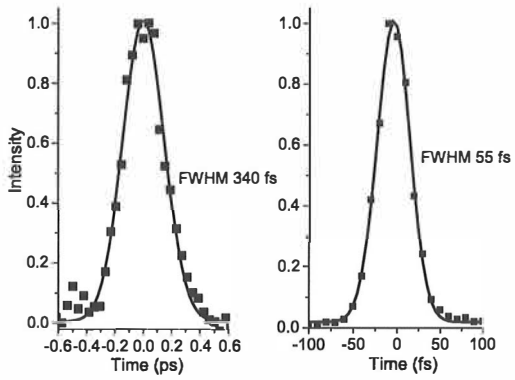

Figure 2.8: Instrument response functions recorded using optical Kerr effect in ethanol solution (left panel) and Cross-correlation in 0.1mm BBO crystal (right panel).

when it becomes shorter wavelength dependent phase information becomes important. A chirped excitation pulse may initiate unwanted processes that overlap in time with the signal of interest. On the other hand, with a designed chirp it is possible to control the outcome of events after excitation into a desired direction. In the present work two methods were employed to obtain instrument response of the system, namely second-harmonic cross-correlation in a non-linear crystal (BBO) and the optical Kerr-effect in ethanol solution (see figure 2.8).

2.4.1 Second-order correlation

Autocorrelation and cross-correlation signals are recorded by spitting a single beam into two and recollecting the beams in a non-linear crystal in a symmetric non-collinear configuration to generate a second harmonic beam (SHG) leaving the crystal in between the two initial beams. By delaying one of the pulses with respect to the other an autocorrelation trance may be recorded, from which with assumed pulse shape the pulse duration may be calculated. An important parameter in autocorrelation and cross-correlation measurements is the phase matching bandwidth, which depends on crystal material and crystal thickness and orientation. Too thick crystal may not convert whole spectral bandwidth of pulses at same angle, and may give two short correlation function. On the other hand in cross-correlation measurement thick crystal may give too long response if there is large difference in

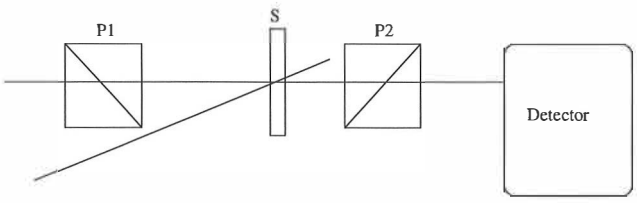

Figure 2.9: Setup for optical Kerr pulse width measurement for a transient absorption experiment.

wavelengths of the pulses due to different speed of wavelengths in crystal.

2.4.2 Optical Kerr effect

Optical Kerr effect is a simple method to measure instrument response of a transient absorption spectrometer. Standard transient absorption setup without any modifications to optical setup before the sample may be used. The only additional optical element needed is a polarizer after the sample (see figure 2.9). Sample is replaced by solvent cyvette or for example glass sheet, and polarizations between pump and detection pulse are set to 45 degree angle to maximize the effect.

It is notable that response of solvents are not instant, but it depends on dielectric properties of mater and for example ethanol solution is well suitable for measuring 100 fs pulses. Thin glass slide has been demonstrated to work with much shorter pulses, This method was used in paper I and in some experiments of paper IV of this work. Optical Kerr gate has been used successfully also for gating fluorescence signals and Raman scattering[111].

2.5 Data-analysis

The importance of data-analysis cannot be underestimated in any time resolved spectroscopy research effort. Basis of a reliable data-analysis is a well performed experiment but even excellent results are worthless without the detailed information obtainable from analysis of good spectroscopic data.

Analysis requires normally the instrument response function in digital form, the recorded kinetic signal and some understanding of what are the main processes in the system under study. Transient signals are normally analyzed using nonlinear least-squares fitting procedure in the time domain[120]. Most common and typically the first method for analysis is the intensity decay law (also called multiple exponential decay method) presented

in Eq. 2.5[120, 121].

$$\Delta A(t,\lambda) = \sum_{i}^{n} A_i(\lambda) \exp(-\Delta t/\tau_i) \tag{2.5}$$

where A_i is the amplitude of a decay component i and τ_i is its lifetime. Δt is time difference between pump and probe pulses. However, to resolve any fast kinetic process comparable to the instrument response, data has to be deconvoluted in the analysis, or more common way is reconvolute model function (f(Δt)) with instrument response (i(Δt)).

$$c(\Delta t) = f(\Delta t) * i(\Delta t) \tag{2.6}$$

2.5.1 Instrument response function and convolution

As described earlier, the instrument response of the experiment gives an upper limit of the rate of a process that can be detected. This means that kinetic traces of all fast events are at least partially perturbed by the finite widths of the auto- or cross-correlation functions. In the data-analysis instrument response function (IRF), if known, can be subtracted from the experimental data. If IRF is known precisely it can be used in the deconvolution process to obtain 'response free' kinetic constants. Deconvolution works nicely only for smooth data. For this reason it is more convenient to convolute the fitting function with IRF. Convolution can be done either analytically or numerically.

If we assume that the instrument response has Gaussian envelope, the analytical convolution with exponential decay can be written as

$$c(t;k,\mu,\Delta) = \frac{1}{2}\exp(-tk)\exp\left(k\left(\mu + \frac{k\tilde{\Delta}^2}{2}\right)\right)\left\{1 + \mathrm{erf}\left(\frac{t-(\mu+k\tilde{\Delta}^2)}{\sqrt{2}\tilde{\Delta}}\right)\right\} \tag{2.7}$$

where k=$1/\tau$, $\tilde{\Delta} = \sqrt{2}\Delta$ means FWHM of the Gaussian response, and μ is the time shift parameter.

In some cases, analytical form of the function c(t;k,μ,Δ) is not known. Then numerical convolution has to be used. Numerical convolution requires equally spaced data for input both for the signal and the response function. There are multiple ways to transform the initially recorded data in such form. Most common is to use interpolation to produce the 'missing' experimental data points. Interpolation of noisy data may generate artifacts like oscillations, amplify noise, result in loss of information, but also weight of the original data will be weakened. In the following another approach

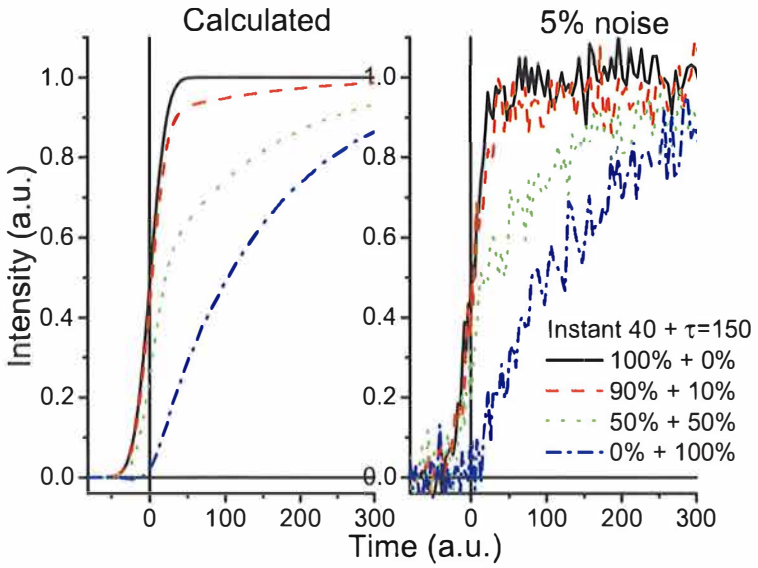

Figure 2.10: Zero-delay with different amount of instant rise.

is described. In the fitting process a multi-exponential function that is assumed to describe the observed kinetics is numerically convoluted with the experimental instrument response function or with a smooth Gaussian. This smooth function is then interpolated to the stepping of the experimental data and residue is calculated. Then this residue is minimized until best fit to the experimental data is obtained. Advantage is that numerical convolution does not depend on type of functions used to model data, like damped oscillations or Gaussians. It can be also used for fittings based on assumed kinetic models, where differential equations need to be solved.

In figure 2.10 three different situations, where Gaussian instrument response function with FWHM of 40 has been used, are shown. The importance of exact positioning of zero-delay point (Δt=0) can be clearly seen in the figures in cases where there is only a small amount of instant rise.

2.5.2 Oscillatory signals

Oscillating signal can be fitted using additional function 2.8 together with the sum of exponentials in the expansion. For signals containing coherent oscillations only numerical convolution of the instrument response is possible.

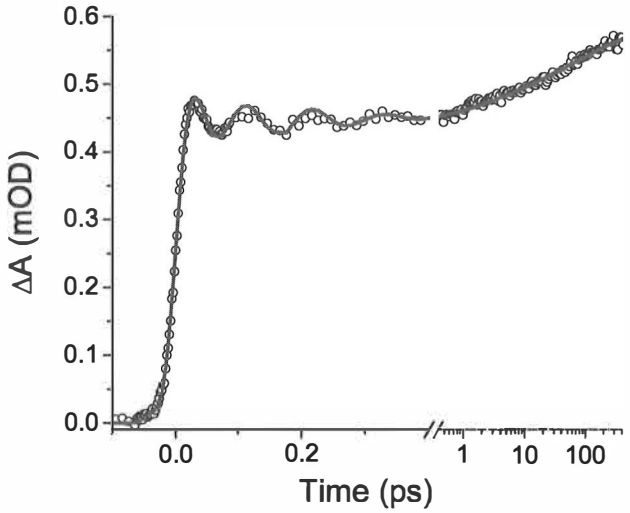

Figure 2.11: Example of fitted oscillations recorded from RuN3-TBA dye on TiO_2 film.

Example of oscillatory behavior in transient absorption signal is in figure 2.11.

$$I = A * \cos(2\pi\omega t + \phi)\exp(-t/\tau) \tag{2.8}$$

where A is amplitude, ω is frequency, ϕ is phase and τ dephasing time of the oscillation.

2.5.3 Global fitting

In a global fitting procedure, a set of data collected at different probe wavelengths is analyzed simultaneously by using an assumed kinetic model of the system under study. For this purpose a program that allows for model testing, including numerical solver for differential equations has been developed. The information one obtains from global fits, is the amplitude distributions of the decay associated spectra (DAS) as function time within the kinetic model. DAS do not always contain direct information about the time behavior of the absorbing species under study, but in some cases it does (See Paper VI, figures 5-7).

2.6 Laser systems used in this work

In this work I have used five different fs-laser systems. Laser System 1 (LS1) had a time-resolution of 100 fs. It consisted of a regeneratively amplified 1 kHz Ti-Sapphire pump laser, a TOPAS (Traveling-wave Optical Parametric Amplifier of Superfluorescence) and a white light continuum probe (Papers I and IV). Laser System 2 had a time-resolution of 35 fs, and it consisted two non-collinear optical parametric amplifiers pumped by a common regeneratively amplified Ti-Sapphire pump laser working at 1 kHz (Papers II, III, IV and V). The experiments where LS2 was used were carried out at the Chemical Physics department of Lund University in co-operation Prof. Villy Sundström. Laser System 3 had a time-resolution of 150 fs and included UV excitation and mid-infrared probing (Paper VII). Laser System 4 consists of two non-collinear OPA's, with time resolution of 45 fs. This laser system was used to perform initial experiments in paper VI and results of Chapter 3. Laser System 5 in paper VI had a time resolution of 25 fs. The measurements were carried out at the Physics Department of the Polytechnico di Milano in co-operation with Prof. Giulio Cerullo and within LASERLAB EUROPE large scale facility program. In this system excitation was generated at about 400 nm and sub-10 fs probe pulses were used over the visible region. Excitation pulses were generated by using second harmonic generation of the output of the pump laser. A single array detector with 1024 pixels was used to detect the broad spectrum of the sub 10 fs pulses as a function of time after excitation.

Chapter 3

Samples

In this chapter we discuss the photophysical properties of the dye molecules studied in this thesis in more detail. First photophysical properties of the most commonly used metal containing sensitizer $Ru(dcbpy)_2(NCS)_2$ will be discussed. Then organic aminophenyl acid sensitizers will be introduced. Finally, excitation energy flow in $Fe(acetylacenonate)_3$ is discussed based on the results obtained from UV excitation mid-IR probe femtosecond experiments (Paper VII).

3.1 $Ru(dcbpy)_2(NCS)_2$-Sensitizer

$Ru(dcbpy)_2(NCS)_2$[122] (RuN3; dcbpy = 4,4'-dicarboxy-2,2'-bipyridine) dye (molecular structure of the dye is shown in figure 3.1) is one of the most efficient and long lasting sensitizers tested in functional solar cells[123]. It has been shown that electron injection efficiency of the dye when attached to nanocrystalline titanium oxide film is nearly unity over the main absorption band[18, 96]. RuN3 dye has a broad absorption spectrum covering most intensive part of the solar spectrum (see figure 1.2). The lowest energy absorption band has a maximum at 538 nm (see figure 3.2).

3.1.1 Electronic structure

Electronic structure of the RuN3 dye has been studied by using semiempirical and recently density functional theory methods and photoelectron spectroscopy[55, 124–129]. In simplistic terms the lowest energy transition can be described as a metal to ligand transition. The highest occupied molecular orbitals of RuN3 contain contributions mainly from d electrons of the metal and electrons of the thiocyanine groups while the lowest unoccupied

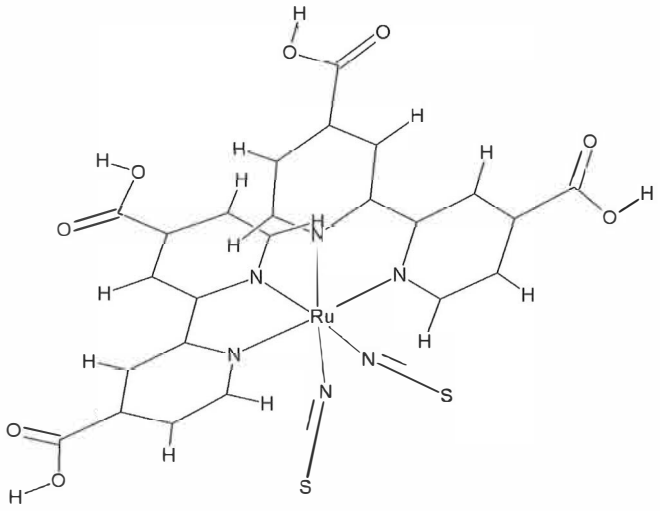

Figure 3.1: Structure of $Ru(dcbpy)_2(NCS)_2$ dye.

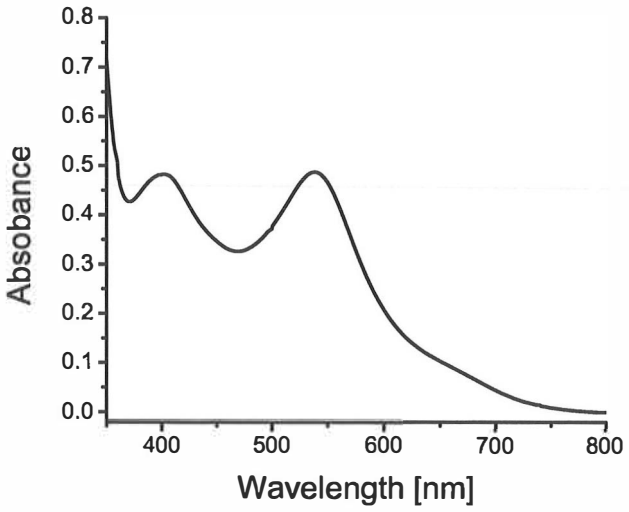

Figure 3.2: Absorption spectrum of $Ru(dcbpy)_2(NCS)_2$ dye on TiO_2 film.

molecular orbitals contain contributions from electrons of the bipyridyls[124–126]. The lowest triplet state has been reported to be about 0.2 eV below the lowest excited singlet state. It is known that in organo-ruthenium complexes, where d-orbitals of the metal are involved in the charge transfer transitions, spin - orbit coupling may mediate efficient crossing of singlet excitation to the triplet manifold. Protonation state of the dye may affect the nature of the lowest excited states. Monat et al. found that in a fully deprotonated ruthenium complex the main absorption of the compound originates from transitions between bipyridyl states[55]. These results are not necessarily fully valid for the protonated RuN3. Guillemoles et al. have performed ground and excited state calculations for the dye without carboxylic acid groups, and found out that all visible transitions have MLCT character[130], and similar results have been obtained from TD-DFT calculations for fully protonated RuN3 dye[1].

3.1.2 Excited state dynamics

The lifetime of the excited state of RuN3 in ethanol solution has been reported to be few tens of nanoseconds[122, 131]. A typical of excited state relaxation channel of the compound has been shown to be an ultrafast intersystem crossing with a time constant of 75 fs[68, 93, 100]. Bhasikuttan and Okada used fluorescence up-conversion to study wavelength dependence of ISC rates [70]. They found wavelength dependent emission lifetimes varying from 43 fs at 600 nm up to 162 fs at 700 nm and proposed a model where the molecule undergoes a cascade type relaxation along a manifold of singlet states with competing ISC taking place in parallel. Several transient absorption studies have been reported on the excited state relaxation processes of the dye [96, 100, 132, 133]. Waterland and Kelley[132] excited the dye at 520 nm and 650 nm and probed the dynamics with probe pulses having center wavelength of 770 nm. The kinetic results were interpreted in terms of a model where the two bipyridyl ligands have different excited state energies and that relaxation from the upper level to the lower level is strongly solvent dependent process. No systematic kinetic studies over the excited state absorption spectrum of the dye extending from 700 to 1100 nm have been published. Such background information is relevant in search for correct wavelengths for monitoring of cation formation on nanocrystalline TiO_2 surface. Transient spectra of RuN3 in ethanol at different delays are shown in figure 3.3. At sub-ps delays two isobestic points in the spectra, one around 850 nm and one around 1000 nm can be identified. At later time the

[1]Private communication with Dr. Petter Persson.

Probe (nm)	80±5 fs	240±30 fs	2.6±0.4 ps	23±2 ps
630	25 % (r)	16 % (r)	3 % (r)	30 % (d)
700	50 % (r)	5 % (r)	29 % (r)	16 % (r)
810	20 % (d)	9 % (r)	2 % (r)	30 % (r)
865	0 % (-)	0 % (-)	7 % (r)	4 % (d)
930	18 % (d)	7 % (d)	5 % (d)	70 % (d)
1030	50 % (r)	10 % (d)	8 % (d)	3 % (d)

Table 3.1: Fitting results obtained from the global analysis of the kinetic traces in figure 3.5.

isobestic points become blurred due to vibrational and solvent relaxations. The main ESA band initially centered around 705 nm shows a red-shift (See figure 3.4) with a time-constant of 23 ps, which is assigned to solvent relaxation of the lowest excited triplet state. Excited state dynamics at various probe wavelengths are shown in figure 3.5. Analysis of the recorded kinetic traces using global fitting procedure gave results that are listed in table 3.1[2].

The resolved 80 fs relaxation process is assigned to electronic conversion, most probably ISC from the initially excited singlet states to the triplet manifold. The 240-fs time constant equals that obtained for the damping of coherent oscillations observed in the early part of the decay signal and is tentatively assigned to wave-packet dynamics between the singlet and triplet states. The 2.6 ps probably reflects intra-complex relaxation to lower energy states. Excitation of the red side of the RuN3 absorption (paper IV) results in a rise with substantial portion being pulse limited and no additional rise components. This was considered as evidence of direct triplet excitation that may become allowed due to mixing of singlet and triplet states of the ruthenium centered complex (figure 2, paper IV).

In Paper III where excited state dynamics of RuN3 was studied in solution and attached to TiO_2 it was suggested that increase in anisotropy in about 20 ps probed at 850 nm is connected to inter-ligand energy transfer (ILET) between bipyridyl ligands. After publication of this paper more detailed dynamics of RuN3 in solution became available (Table 3.1.) and it was observed that a 23 ps spectral evolution observed around 700 nm was due to solvent relaxation (See figures 3.3 and 3.4) which could not be seen at the isobestic point of the ESA spectrum around 850 nm. Since in the ground state the bipyridyl ligands of RuN3 in solution are equivalent, there is now

[2] All transient signals at each probing wavelength in figure 3.5 decay with »10 ns lifetime to zero. If the rise amplitudes of table 3.1 are not summed up to 100%, there is instant part in signal. (r) = rise, (d) = decay.

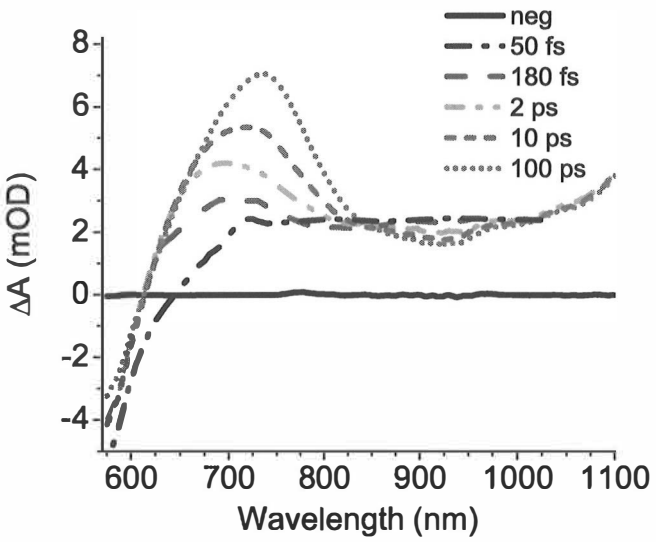

Figure 3.3: Transient absorption spectra of Ru(dcbpy)$_2$(NCS)$_2$ in ethanol solution over excited state absorption region.

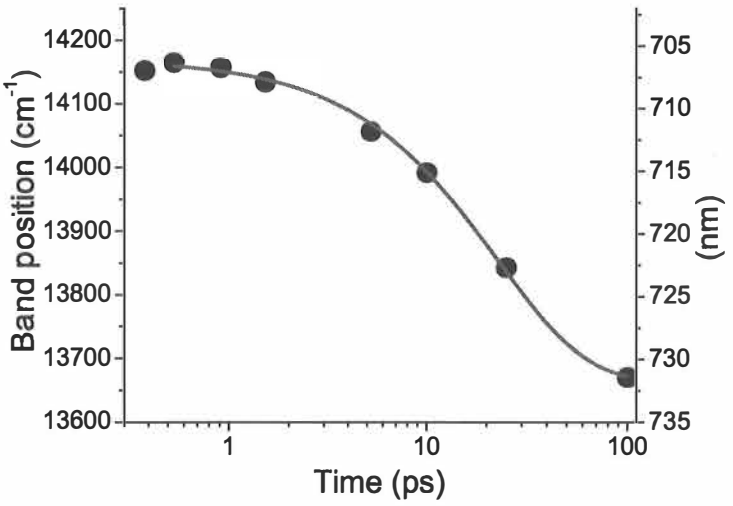

Figure 3.4: Time dependence of the red-shift of the exited state absorption of Ru(dcbpy)$_2$(NCS)$_2$ in ethanol solution after excitation.

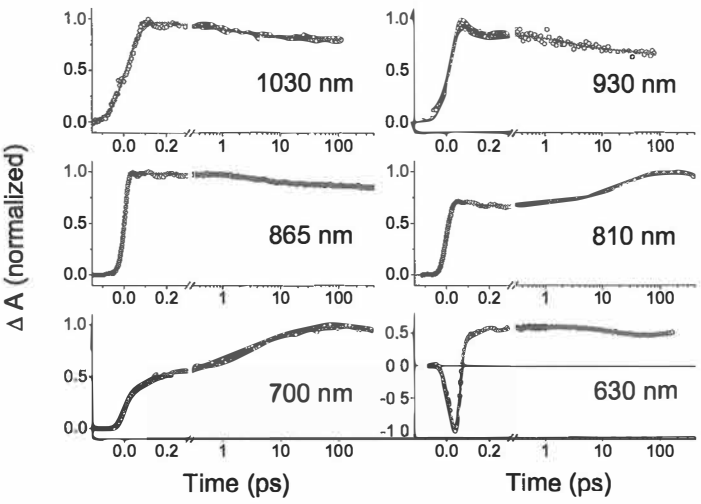

Figure 3.5: Excited state dynamics recorded from RuN3 in ethanol solution at various probe wavelengths after 535 nm excitation.

way of saying which of the two preferably will be excited or both. Assuming that only one of the ligands receives excitation then excited state solvent relaxation around this ligand will take place and its energy is reduced with respect to the non-excited ligand.

The observed increase of negative anisotropy around 850 nm, where solvent shift is not visible, then must be explained not as ILET, but as interplay between two excited state absorption transitions with different directions of ESA transition dipole moments. As a result of solvent relaxation changes in the ligand coordination can change the direction and magnitude of the transition dipole during solvent relaxation (MC transitions) as has been reported for $Ru(bpy)_3^{2+}$ [134]. However, since not all ligands in the RuN3 are identical reorganization may open a channel for ILET between different ligands as seen for example as a minor 16 ps component for $Ru(bpy)(py)_4$ in solution [134].

3.1.3 Electron transfer

Electron transfer from the RuN3 dye to conduction bands of different oxide semiconductors has been studied by femtosecond transient absorption spectroscopy by several groups. Main focus of research has been on the RuN3-

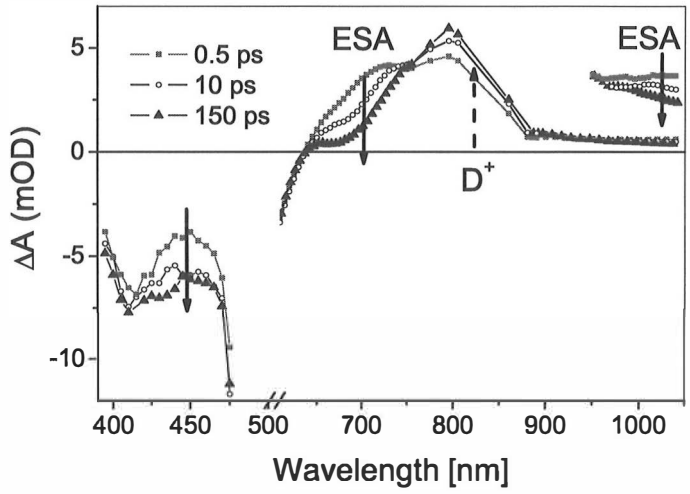

Figure 3.6: Transient absorption spectra of Ru(dcbpy)$_2$(NCS)$_2$ on TiO_2 over visible and NIR region[93].

TiO_2 system that has shown nearly unity injection efficiency in functioning solar cells [18]. A number of studies suggest that the electron injection process is multi- phasic[I][17, 68, 93, 96, 98–100, 109, 133, 135, 136]. To explain the multi-exponential injection kinetics a model including sub 100 fs singlet injection (about60%) and a multiexponential from 5 to 100 ps component (about 40%) reflecting triplet injection has been presented[I],[68, 93]. It has also been suggested that the picosecond injection results from aggregation of the dye on the semiconductor surface [99]. In this study partially deprotonated analogue of the RuN3 dye (N719) was used as the sensitizer and the results were compared to fully protonated RuN3 sensitizer. The mechanisms of picosecond injection are discussed in more detail in Paper V.

Electron injection from RuN3 to other nanocrystalline semiconductor materials like ZnO[97, 137] and SnO_2[II,III,IV],[133] have been studied as well. Injection efficiencies and electron transfer rates in these semiconductor films do not significantly differ from electron transfer taking place in sensitized TiO_2.

Dye	NK1	NK2	NK7
Abs (EtOH)	412 nm	416 nm	417 nm
ε	30000	13900	25000
Efficiency	4.7%	4.1%	2.4%

Table 3.2: Physical properties of NK-dyes.

3.2 Aminophenyl Sensitizers

In paper VI electron transfer from three blue absorbing organic sensitizers was studied. Molecular structures of the dyes are shown in figure 3.7. The dyes 2E,4E-2-Cyano-5-(4-dimethylaminophenyl)penta-2,4-dienoic acid (later referred as NK1), 2-[(E)-3-(4-dimethylaminophenyl)-allylidene]malonic acid (NK2) and 2E,4E-2-Cyano-5-(4-diphenylaminophenyl)penta-2,4-dienoic acid (NK7) were received from Nippon Kayaku Co., Ltd, Japan[108]. As light harvesters in solar cells, these dyes have shown light to current efficiencies ranging from 3% to 5% [108]. Electron injection rates of these dyes have not been reported earlier. Similar dyes having shorter conjugated chains have been studied by using vis-mid-IR transient absorption spectroscopy. A single exponential sub-100 fs electron injection rate from these studies has been reported.

Amino-phenyl dyes show characteristic spectral properties when attached to TiO_2 and to high band gap semiconductor Al_2O_3 films. From sensitized TiO_2 films no fluorescence was seen while in Al_2O_3 fluorescence intensity was nearly the same as the intensity seen from solution, which suggests that efficient electron injection takes place from the sensitizer to TiO_2. The shifts of the absorption band maxima of the lowest energy transitions of the dyes when attached to TiO_2 or Al_2O_3 do not show any systematic behavior an indication of characteristic dye - semiconductor interactions [VI]. According to DFT calculations excitation of the lowest energy transitions of these dyes induces a charge transfer towards the carboxylic groups from where the dyes are bound to the semiconductor nanoparticles. Calculations also showed that the dye cations absorb in very different spectral regions than the neutral species [VI]. It is known that the dyes form aggregates in solution and hence assumingly also on nanocrystalline semiconductor surfaces. A known co-adsorbate was used in all sample preparation to prevent aggregation. Physical properties of the dyes, obtained from the manufacturer, are listed in the table 3.2.

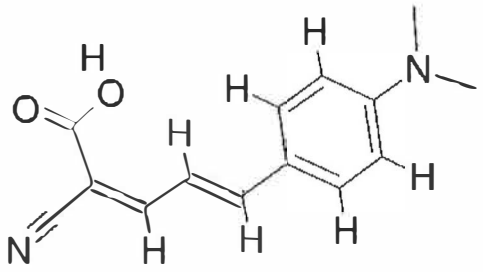

NK 1

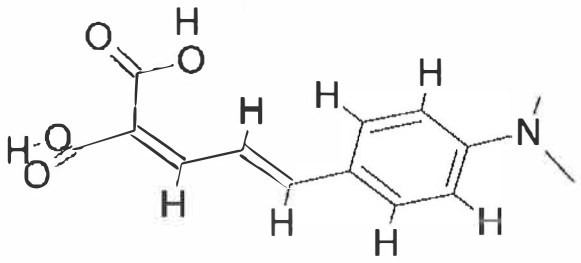

NK 2

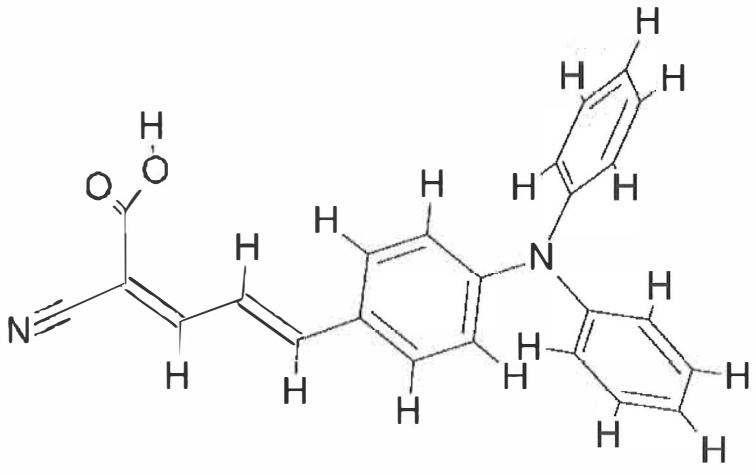

NK 7

Figure 3.7: Structures of NK1, NK2 and NK7 dyes

3.3 Preparation of the dye/semiconductor samples

All RuN3 samples were prepared as described in reference [138] without further modifications. For organic amino-phenyl dyes solvent 3-metoxy-propionitrile was used because it is less volatile than acetonitrile. Tin dioxide and aluminum oxide pastes were prepared as reported in the literature[136, 139].

Porous nanoparticle films of thickness of 2-3 micrometers were prepared by spreading the semiconductor nanoparticle paste on top of a microscope cover slide by rolling a glass rod on top of a Scotch Magic tape frame. Films were sintered under hot air at 450 ^{o}C for 15 minutes to attach the nanoparticles on a glass substrate, and to create contacts between nanoparticles. After cooling the films to 80 ^{o}C they were placed in a dye bath (for RuN3 solution for several hours and for organic sensitizers for few minutes). Parafilm frame was used to seal the solvent in between the active electrode and the thin glass cover slide both held together with paper clamps.

3.4 Fe(acetylacetonate)$_3$ complex

The complex Fe(acetylacetonate)$_3$ was considered as a good model system to study excited state relaxation channels of a non-reacting complex in solution. The ligands of this complex become negatively charged in aprotic solutions, giving rise to the non-reactive character of the compound in solution. Hence electronic conversion, vibrational relaxation and transfer of excess excitation energy to the solvent bath may be studied without interference from photoreactions. The Fe(acac)$_3$ complex contains a large number of vibrational degrees of freedom and hence fast vibronic relaxation is expected.[3]

Fe(acac)$_3$ has strong electronic absorption bands at 270, 350 and 440 nm which have been assigned to pi - pi, metal to ligand and ligand to metal charge transfer transitions, respectively. The complex has two characteristic absorption bands in the infrared spectrum one at 1525 cm^{-1} (CC stretch) and one at 1575 cm^{-1} (CO stretch). These vibrational bands were used to probe the transient absorption changes after excitations at 340 and 400 nm. The experimental mid-infrared setup was built over several months and used for the first time in these experiments. For experimental details we refer to Paper VII.

[3]Fe(acac)$_3$ has 123 degrees of vibrational freedoms, and density of states increases drastically with increasing excess energy.

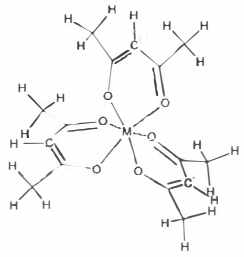

Figure 3.8: Structure of acetonate dye

An immediate bleach of the ground state molecule was observed after both excitations. The bleach recovered with a characteristic time constant of 8 to 20 ps depending on the excitation wavelength and the solvent. No signs of permanent photoproducts were observed. Besides the bleach of the ν(C=C) and ν(C=O) bands, positive absorption signals on the red side of these bands, typical signatures of population of hot vibrational states, were identified (see figure 3.9). These red shifted bands showed time dependent peak maxima shifts and half widths, with typical time constants from 3 to 9 ps. It was concluded that after UV excitation Fe(acac)$_3$ in solution reaches a charge transfer state that experiences electronic conversion to a lower lying vibrationally hot electronic state, a spin flip state. In this state mode selective vibrational cooling takes place after which again electronic conversion to the ground state occurs in about 8 to 15 ps. Some evidence was obtained for mode specific vibrational energy transfer into the surrounding solvent bath [VII].

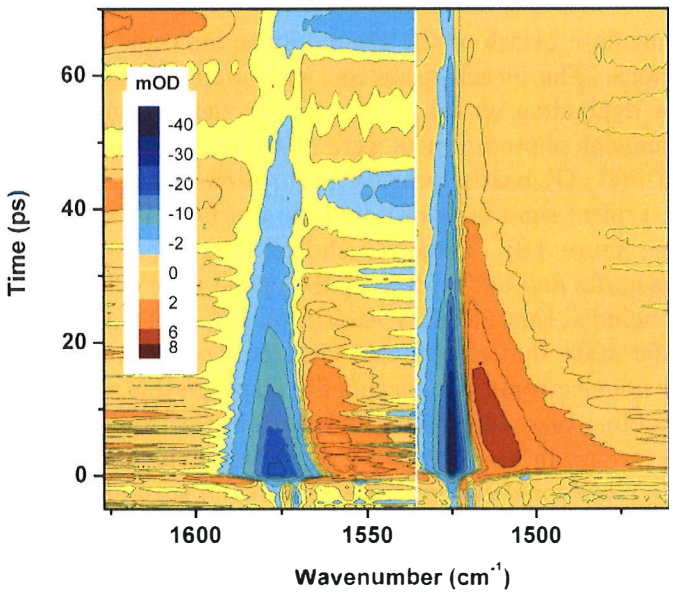

Figure 3.9: Bleach recovery and vibrational cooling signals of $Fe(acac)_3$ in tetrachloroethylene after 400 nm excitation seen by ν(C=C) and ν(C=●) modes probed in the mid-infrared region.

Chapter 4

Electron transfer - Results and discussion

In this chapter main results of the Thesis considering electron transfer are summarized. Most of the work focused on efforts to understand the underlying photophysical reasons of the picosecond electron injection in RuN3 sensitized nanocrystalline TiO_2 thin films, the active electrode of the most efficient known dye sensitized solar cell (Papers I-V). In addition results on electron injection from organic aminophenyl dyes to TiO_2 are reported. In these measurements sub 20 fs time resolution was needed (Laser System 5, Paper VI).

In paper I it was convincingly demonstrated for the first time that electron injection from excited states of the RuN3 dye to TiO_2 nanocrystalline film contained not only a fast sub 100 fs component but non-exponential picosecond components (1-100 ps) which could be related to formation of the dye cation. The fundamental observation was that the excited state absorption decay observed around 700 nm was found to match the picosecond rise resolved at wavelengths longer than 750 nm. Three characteristic picosecond time constants 1, 12 and 100 ps were obtained from Global analysis of the data. The final assignment of the measured picosecond kinetics to electron injection in TiO_2 films was based on reference measurements under similar experimental conditions for RuN3 in solution and attached to the high band gap non-injecting nanocrystalline Al_2O_3 thin film. These samples showed a pulse limited rise and a flat, long lived » 100 ps transient absorption signal and no wavelength dependence.

To build up a detailed photophysical picture of the apparently heterogeneous electron injection, both the fast sub 100 fs and the slow ps processes, it was realized that much better time resolution than was available in our laboratory was needed. The early observations in Jyväskylä served as a trig-

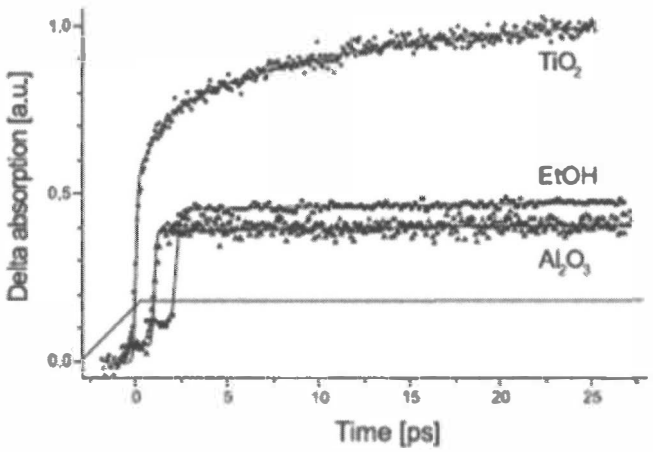

Figure 4.1: Picosecond electron injection in RuN3 sensitized nanocrystalline TiO_2 film. Reference signals for RuN3 in solution and attached to non-injecting Al_2O_3 nanocrystalline film (figure from Paper I).

ger for co-operation with Prof. Villy Sundström, at Chemical Physics of the University of Lund and consequently a series of joint investigations was to follow. Time resolution of 30 fs was finally needed in the measurements, which allowed building up the final injection model, where 60% of the injection was shown to occur from non-thermalized singlet charge transfer states at exceedingly fast rate of 50 fs and the rest 40% after inter system crossing from triplet states at non-exponential picosecond rates already resolved in Paper I[68, 93].

Paper II reports first efforts towards understanding the origin of the heterogeneity of electron transfer in RuN3 sensitized nanocrystalline semiconductor films. In this work injection kinetics of RuN3 attached to two different semiconductor materials TiO_2 and SnO_2 was studied. It was observed that singlet injection rates were dependent on the semiconductor, being 55 fs in TiO_2, in accord with the previous measurements, [68, 93] and 145 fs in SnO_2. This result indicated that the driving force of electron injection is not only due to the energy difference between the LUMO of the sensitizer and the conduction band edge of the semiconductor as reported before [100, 137] but it seemed plausible that also the coupling strength between the dye and the semiconductor states plays a role in electron injection as well as the density of states above and below the conduction band edge of the semiconductor. Justification of the argument came from the fact that

the conduction band edge potential of SnO_2 is 0.4 eV more positive (lower in energy) than that of TiO_2. A surprise was also that the picosecond injection kinetics in these semiconductors were almost identical, independent of the facts that the semiconductors have different conduction band edge energies and that SnO_2 has lower density of states than TiO_2. Tentatively it was suggested that possibly internal excited triplet state kinetics of RuN3 drives the slower, non-exponential picosecond injection. It is pointed out that in the studied system no electrolyte was used and hence any effects due to adsorption of the electrolyte cation on the TiO_2 surface, known to reduce the conduction band edge energy[33, 34], were not present. In the functioning cell such effects become important but these were not studied in this paper.

The experiments of Paper III were designed to shed light to triplet excited state dynamics of the RuN3 sensitizer prior to slow electron injection. The same semiconductor films as in Paper II were sensitized with RuN3 and measurements were carried out in two different solvents, acetonitrile and ethanol. A clear solvent dependence of picosecond electron transfer was observed, injection being slower in sensitized films imbedded in ethanol than in acetonitrile, in particular the amplitude of the 1 ps component was reduced and that of the 80 ps component increased in ethanol as compared to acetonitrile. This was interpreted as RuN3 excited triplet - solvent interaction. To test the idea that inter-ligand charge transfer is responsible of the slow injection electron injection dynamics of the Ru520DN sensitized TiO_2 films were investigated. This dye has only two carboxylic groups that can attach to semiconductor particles as compared to four of RuN3. It was thought that if the injection dynamics of the two dyes on the same semiconductor were the same then it could be concluded that when RuN3 binds to TiO_2 only two carboxylic groups are involved. The results for Ru520DN gave support to the interpretation that RuN3 really uses only two of its carboxylic groups for binding to TiO_2 meaning that the two non-binding carboxylic groups are energetically different as compared to the ones that bind. Anisotropy measurements at 850 nm for RuN3 in solution and on TiO_2 revealed the expected fast sub 100 fs dynamics, 65 fs for the solution typical of ISC and 30 fs for the injecting system. For RuN3 in solution a delayed exponential decrease of anisotropy with a time constant of about 20 ps was observed and assigned to inter ligand electron transfer (ILET). For the RuN3 dye attached to TiO_2 and SnO_2 this component was also observed but fitting needed three time constants, roughly the same as observed in the region of RuN3 cation formation in the magic angle pump - probe experiment. This was considered as strong evidence for excited non-bonded bipyridyl of the RuN3 being responsible of driving the picosecond electron injection. The interpretation holds the assumption that injection from the bound bipyridyl ligand of RuN3

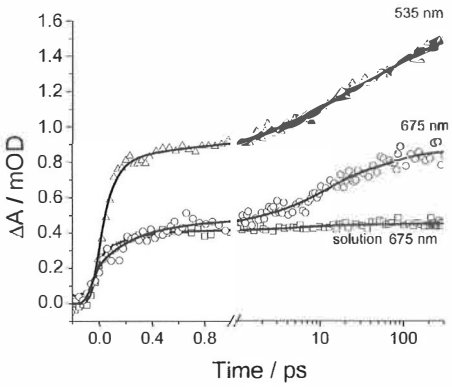

Figure 4.2: Triplet and cation formation of RuN3 in solution and attached to TiO_2 after 535 and 675 nm excitations (Figure from Paper IV).

occurs in 50 fs or faster.

In Paper IV further justification of presence of triplet injection was obtained. Again both TiO_2 and SnO_2 semiconductor films were sensitized with the RuN3 dye. Now the leading idea was that singlet and triplet states of the dye are mixed and that the triplet absorption is an allowed transition and the triplet states could be directly populated by exciting in the red wing of the RuN3 absorption band. If this was the case then only picosecond electron transfer should be observed. To get evidence for direct population of the triplet state(s) of RuN3 in solution excitation wavelengths of 535 and 675 nm and probe wavelength of 1020 nm were used. It was clear that the excited state triplet rise at 1020 nm was much faster for 675 nm excitation than for 535 nm excitation, the difference being the time delay caused by ISC in the latter case. The experiment showed that red wing excitation directly populates the triplet manifold of RuN3 while excitation at absorption maximum populates the triplet via ISC. The next step was to monitor cation formation at 860 nm with 535 and 675 nm excitations on the sensitized TiO_2 film and triplet absorption rise of RuN3 in solution at the same wavelength (Figure 4.2). It became clear that in the time window up to one picosecond at 675 nm excitation formation of triplet is seen for both solution and RuN3 attached to TiO_2. After one picosecond rise components of 5, 30 and 180 ps were resolved indicative of cation formation from triplet states. Comparison to 535 nm excitation reveals the fast sub 100 fs cation formation as increased amplitude on top of the triplet rise signal. It was possible to estimate from the signals that at 675 nm excitation electron injection is about 40% lower

than with 535 nm excitation (singlet injection not activated). Lower triplet injection efficiency was interpreted arising from energy relations between the populated triplet states and the conduction band states of TiO_2. Triplet states near but below the conduction band would inject less efficiently than the states above the conduction band. The idea was tested by exciting the triplets at several wavelengths from 620, 650 and 675 nm and by looking picosecond formation of the RuN3 cation at 860 nm. Clear slowing down of injection rates was observed when excitation moved towards red, indicating that it is harder for electrons to become injected from states below the conduction band. No such wavelength dependence was observed for injection from red excited RuN3 sensitized nanocrystalline SnO_2 films, an expected result since the conduction band edge potential of SnO_2 is 0.4 eV lower than that of TiO_2.

It has been suggested that aggregation not triplet injection is the reason for the slow picosecond electron transfer discussed above.[99] To test the presented hypothesis experiments for the protonated form of RuN3 and partly deprotonated tetrabutylammonium salt of RuN3 (RuN3-TBA, also known as N719) were made in solution and the dyes attached to TiO_2(Paper V). One of the key findings was that the excited state absorption spectra of the two dyes in solution are blue shifted almost 50 nm with respect to each other as well as the cation absorbing spectral regions (See Paper V and figure 4.3).

The practical consequence of this finding was that cation absorption of RuN3-TBA should be probed at 810 nm, fifty nanometers towards blue from the isobestic point of RuN3 located at 860 nm. The next step was to monitor the picosecond injection kinetics of the two dyes at appropriate wavelengths. For both dyes surprisingly similar picosecond kinetics, yet with varying amplitudes, were obtained. An explanation to the contradicting, previously published results could be given. Durrant and co-workers[140] reported from 1 to 500 ps injection from RuN3-TBA to TiO_2 by probing at 760 nm the absorption region of the cation, while Moser and co-workers[99] reported no picosecond injection when probing at 860 nm. From the transient spectra of RuN3-TBA attached to TiO_2 it is seen that only a fractional absorption change of RuN3-TBA cation can be seen at 860 nm. In addition, sample films sensitized from several dye solutions with varying dye concentrations revealed that the picosecond injection components were present even in samples made from the most dilute solution, when dye aggregation is not expected to take place. A further finding was that increasing pump intensity has a tendency to suppress the amplitude of the picosecond injection which could add to the difficulty of seeing traces of RuN3-TBA cation absorption at 860 nm.

In Paper VI blue absorbing dyes, aminophenyl sensitizers, were stud-

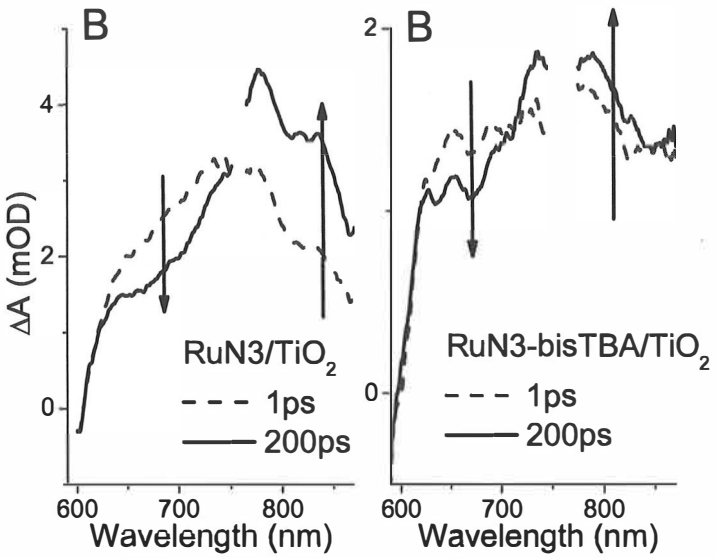

Figure 4.3: Transient absorption spectra of RuN3 and RuN3-TBA on titanium dioxide film at two time delays (Figure from Paper V).

ied as potential electron donors on nanocrystalline TiO_2 films. Two of the dyes have the same conjugated backbone but different number of anchoring carboxylic groups, the NK1 dye one, the NK2 dye two. The third dye NK7 possesses one carboxylic group but the amine periphery contains two benzene rings instead of two methyl groups in the other two dyes (see figure 3.7). For the two first mentioned dyes 5% light to electricity conversion efficiency had been demonstrated in a functional dye sensitized solar cell, while for the third dye only 2.4% efficiency has been reported. One of the aims of the study was to try to find the underlying reasons for the different efficiencies. The three dyes attached to TiO_2 were not fluorescent, while solutions and sensitized Al_2O_3 films showed equally strong fluorescence spectra. The femtosecond dynamics of the dyes were studied in solution and attached to TiO_2 and Al_2O_3 nanocrystalline films. For excitation 20 fs blue pulses centered at 450 nm and a broad band probe pulse from 500 to 700 nm with pulse duration of about 7 fs were used in pump probe experiments. TD-DFT calculations were used to reveal that the NK1 and NK2 dye cations absorb in the red part of the visible spectrum beyond 650 nm, while the NK7 cation was expected to absorb around 550 nm. The NK1 and NK2 dyes showed stimulated emission signals in the wavelength region probed. The dyes attached to TiO_2 showed stimulated emission decays of sub 30 fs and sub 300 fs at 580 nm while in Al_2O_3 the corresponding time constants were about 100 times longer. The fast time components could be resolved as rise components at 670 nm in the region were the dye cations were predicted to absorb (see Figure 4.4), strong evidence of electron injection taking place in NK1 and NK2 sensitized TiO_2 films. Since the ET kinetics for the NK1 and NK2 dyes were almost identical it was concluded that the number of anchoring groups did not have much influence on electron injection efficiency. For the NK7 dye the transient spectra differ from the other dyes in that photo-induced absorption was observed over the probe spectrum; a narrow excited state absorption at 530 nm was identified and the cation absorption emerged around 550 nm. There was no indication of stimulated emission for the dye. Electron injection with a time constant of 270 fs was seen as a decay of ESA around 530 nm and as the corresponding rise at 550 nm, where the dye cation was predicted to absorb. The early kinetics of the NK7 dye probed at 580 nm for both sensitized TiO_2 and Al_2O_3 films showed a very fast transient with a pulse limited rise and about 40 fs decay (see Figure 4.5) to an intermediate absorption level after which in TiO_2 formation of the cation was seen as a 270 fs rise. The amplitude of the short living transient was four times larger in Al_2O_3 than in TiO_2 and the decay about 25% faster in the latter. This behavior was assigned to excited state isomerization of the two benzene rings present in NK7, to a reaction that competes with electron injection and dissipates part

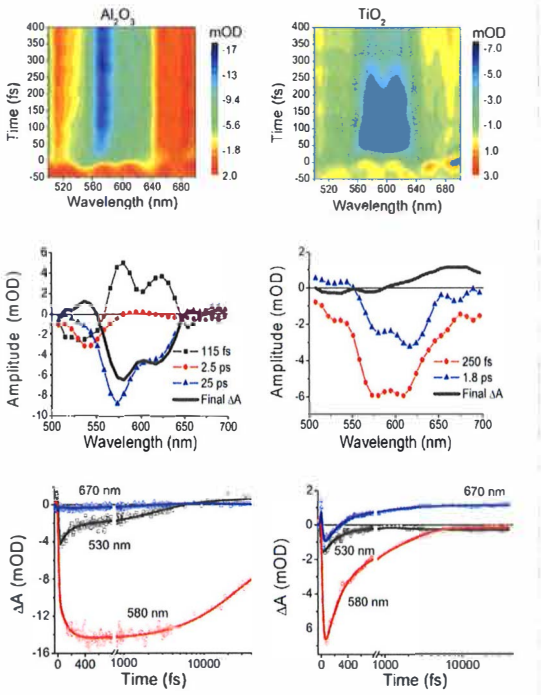

Figure 4.4: Two dimensional transient absorption signals, decay associated spectra and kinetic traces at selected wavelengths for the NK1 dye attached on TiO_2 and on Al_2O_3.

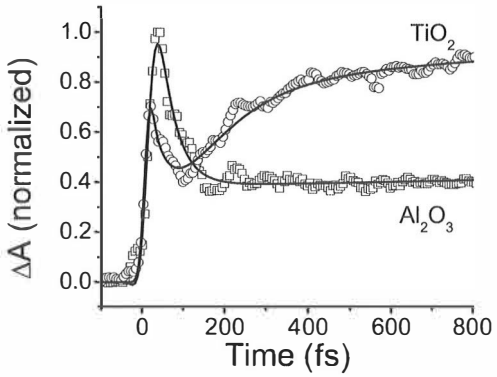

Figure 4.5: Early kinteics of the NK7 dye attached to TiO_2 and Al_2O_3, respectively, recorded at 580 nm probe wavelength (Figure from Paper VI).

of the excitation energy into heat. Such excitation energy distribution may be at least one reason for lower efficiency (as compared to NK1 and NK2) in the NK7 sensitized solar cell. Finally it was concluded that molecular design for organic sensitizers should aim for long conjugation lengths and rigid structures to allow broad spectral absorption and efficient electron transfer.

Chapter 5

Conclusions

Major part of this Thesis work focused on the study of the slow injection channel in RuN3 sensitized nanocrystalline TiO_2 films. After a series of studies it has been established that the slow injection channel provides about 40% of the total injection and that possibly charge transfer from the unbound RuN3 bipyridyl ligand controls the triplet injection. Aggregation of the RuN3 dye was shown to play a minor role in the slow injection. Three organic aminophenyl sensitizer dyes were also studied for their forward electron injection efficiency. For all these dyes very fast injection rates about 30 fs and sub 300 fs were determined. In addition a competing excited state relaxation channel to electron injection was found for the dye with two flexible benzene substituents in the amino terminal group. Finally an iron complex, Fe(acetylacetonato)$_3$ in several solutions was studied by using UV excitation and mid-infrared probe pulses. Bleach recovery to the ground state lasting from 12 to 19 ps in chloroform and tetrachloroethylene were detected by monitoring the time evolution of the absorption by the carbonyl and carbon - carbon double bond stretching modes. Transient spectra showed line narrowing and a blue shift lasting from 3 to 9 ps independent of the solvent. The results were interpreted in terms of fast conversion of the initially excited charge transfer states to the ligand field manifold and subsequent cooling on the lowest ligand field state prior dark relaxation to the ground state.

Bibliography

[1] P. Kamat, J. Phys. Chem. C **111**, 2834 (2007).

[2] S. Günes, H. Neugebauer, and N. S. Sariciftci, Chem. Rev. **107**, 1324 (2007).

[3] M. C. Scharber, D. Mühlbacher, M. Koppe, P. Denk, C. Waldauf, A. J. Heeger, and C. J. Brabec, Adv. Mater. **18**, 789 (2006).

[4] B. O'Regan and M. Grätzel, Nature **353**, 737 (1991).

[5] A. Hagfeldt and M. Grätzel, Acc. Chem. Res. **33**, 269 (2000).

[6] M. Grätzel, Coord. Chem. Rev. **111**, 167 (1991).

[7] K. Kalyanasundaram and M. Grätzel, Coord. Chem. Rev. **77**, 347 (1998).

[8] A. Hagfeldt and M. Grätzel, Chem. Rev. **95**, 49 (1995).

[9] Y. I. Kim, S. J. Atherton, E. S. Brigham, and T. E. Mallouk, J. Phys. Chem. **97**, 11802 (1993).

[10] K. Hara, Y. Tachibana, Y. Ohga, A. Shinpo, S. Suga, K. Sayama, H. Sugihara, and H. Arakawa, Sol. Energy Mater. Sol. Cells **77**, 89 (2003).

[11] H. Gerischer and H. Tributsch, Ber. Bunsenges. Phys. Chem. **73**, 251 (1969).

[12] H. Gerischer and H. Tributsch, Ber. Bunsenges. Phys. Chem. **72**, 437 (1968).

[13] M. Grätzel and K. Kalyanasundaram, *Photosensitization and photocatalysis using inorganic and organomatellic compounds* (Kluwer Academic Publishers, 1993), chap. Metal complexes as photosensitizers in photoelectrochemical cells, pp. 247–271.

[14] M. Gleria and R. Memming, Z. Phys. Chem. **98**, 303 (1975).

[15] G. Meyer, J. Chem. Educ. **74**, 652 (1997).

[16] H. Zabri, F. Odobel, S. Altobello, S. Caramori, and C. A. Bignozzi, J. Photo Chem. Photo Biol. A **166**, 99 (2004).

[17] C. She, J. Guo, S. Irle, K. Morokuma, D. L. Mohler, H. Zabri, F. Odobel, K.-T. Youm, F. Liu, J. T. Hupp, et al., J. Phys. Chem. A **111**, 6832 (2007).

[18] J. E. Moser and M. Grätzel, Chimia **160**, 52 (1998).

[19] K. Hashimoto, M. Hiramoto, and T. Sakata, Chem. Phys. Lett. **148**, 215 (1988).

[20] K. Sayama, S. Tsukagoshi, T. Mori, K. Hara, Y. Ohga, A. Shinpou, Y. Abe, S. Suga, and H. Arakawa, Sol. Energy Mater. Sol. Cells **80**, 47 (2003).

[21] M. K. Nazeeruddin, R. Humphry-Baker, M. Grätzel, and B. A. Murrer, Chem. Commun. **98**, 719 (1998).

[22] J. He, G. Benkö, F. Korodi, T. Polivka, R. Lomoth, B. Åkermark, L. Sun, A. Hagfeldt, and V. Sundström, J. Am. Chem. Soc. **124**, 4922 (2002).

[23] F. Odobel, E. Blart, M. Lagree, M. Villieras, H. Boujtita, N. E. Murr, S. Caramori, and C. A. Bignozzi, J. Mater. Chem. **13**, 502 (2003).

[24] R. Huber, J.-E. Moser, M. Grätzel, and J. Wachtveitl, J. Phys. Chem. B **106**, 6494 (2002).

[25] Z.-S. Wang, K. Hara, Y. Dan-oh, C. Kasada, A. Shinpo, S. Suga, H. Arakawa, and H. Sugihara, J. Phys. Chem. B **109**, 3907 (2005).

[26] C. Zimmermann, F. Willig, S. Ramakrishna, B. Burfeindt, B. Pettinger, R. Eichberger, and W. Storck, J. Phys. Chem. B **105**, 9245 (2001).

[27] A. Morandeira, G. Boschloo, A. Hagfeldt, and L. Hammarstrom, J. Phys. Chem. C **112**, 9530 (2008).

[28] B. O'Regan and D. T. Schwartz, Chem. Mater. **7**, 1349 (1995).

[29] M. Borgstrom, E. Blart, G. Boschloo, E. Mukhtar, A. Hagfeldt, L. Hammarstrom, and F. Odobel, J. Phys. Chem. B **109**, 22928 (2005).

[30] A. Morandeira, G. Boschloo, A. Hagfeldt, and L. Hammarstrom, J. Phys. Chem. B **109**, 19403 (2005).

[31] D. M. Roundhill, *Photochemistry and photophysics of metal complexes* (Plenum Publishing Corporation, 1994).

[32] J. A. Pollard, D. Zhang, J. A. Downing, F. J. Knorr, and J. L. McHale, J. Phys. Chem. A **109**, 11443 (2005).

[33] S. Nakade, T. Kanzaki, W. Kubo, T. Kitamura, Y. Wada, and S. Yanagida, J. Phys. Chem. B **109**, 3480 (2005).

[34] K. Fredin, J. Nissfolk, G. Boschloo, and A. Hagfeldt, J. Electroanal. Chem. **609**, 55 (2007).

[35] A. H. Zewail, J. Phys. Chem. A **104**, 5660 (2000).

[36] Y. Tanimura and S. Mukamel, J. Chem. Phys. **99**, 9496 (1993).

[37] P. Hamm, M. Lin, and R. Hochstrasser, J. Phys. Chem. B **102**, 6123 (1998).

[38] J. Bredenbeck, J. Helbing, R. Behrendt, C. Renner, L. Moroder, J. Wachtveil, and P. Hamm, J. Phys. Chem. B **107**, 8654 (2003).

[39] M. Hentschel, R. Kienberger, C. Spielmann, G. Reider, N. Milosevic, T. Brabec, P. Corkum, U. Heinzmann, M. Drescher, and F. Krausz, Nature **414**, 509 (2001).

[40] M. Kling, C. Siedschlag, A. Verhoef, J. Khan, T. Uphues, Y. Ni, M. Uiberacker, M. Drescher, F. Krausz, and M. Vrakking, Science **312**, 246 (2006).

[41] J. Williamson, J. Cao, H. Ihee, H. Frey, and A. H. Zewail, Nature **386**, 159 (1997).

[42] C. Bressler, M. Saes, M. Chergui, D. Grolimund, R. Abela, and P. Pattison, J. Chem. Phys. **116**, 2955 (2002).

[43] T. Anderson, I. Tomov, and P. Rentzepis, J. Chem. Phys. **99**, 869 (1993).

[44] I. Tomov, D. Oulianov, P. Chen, and P. Rentzepis, J. Phys. Chem. B **103**, 7081 (1999).

[45] C. Siders, A. Cavalleri, K. Sokolowski-Tinten, C. Toth, T. Guo, M. Kammler, M. H. von Hoegen, K. Wilson, D. von der Linde, and C. Barty, Science **286**, 1340 (1999).

[46] G. Cerullo, M. Nisoli, and S. D. Silvestri, Appl. Phys. Lett. **71**, 3616 (1997).

[47] T. Wilhelm, J. Piel, and E. Riedle, Opt. Lett. **22**, 1494 (1997).

[48] G. Cerullo, M. Nisoli, S. Stagira, and S. D. Silvestri, Opt. Lett. **23**, 1283 (1998).

[49] A. Shirakawa, I. Sakane, and T. Kobayashi, Opt. Lett. **23**, 1292 (1998).

[50] A. Shirakawa, I. Sakane, M. Takasana, and T. Kobayashi, Appl. Phys. Lett. **74**, 2268 (1999).

[51] T. Kobayashi, T. Saito, and H. Ohtani, Nature **414**, 531 (2001).

[52] G. Cerullo, G. Lanzani, M. Muccini, C. Taliani, and S. D. Silvestri, Phys. Rev. Lett. **83**, 231 (1999).

[53] T. Kobayashi, *Femtosecond laser spectroscopy* (Springer, 2005), chap. Real-time spectroscopy of molecular vibrations with sub-5-fs visible pulses, pp. 133–165.

[54] N. J. Turro, *Modern Molecular Photochemistry* (University Science Books, 1991), chap. 1, pp. 1–16.

[55] J. E. Monat, J. H. Rodrigues, and J. K. McCusker, J. Phys. Chem. A **106**, 7399 (2002).

[56] A. Juris, V. Balzani, F. Barigelletti, S. Campagna, P. Belser, and A. V. Zelewsky, Coord. Chem. Rev. **84**, 85 (1988).

[57] K. Kalyanasundaram, *Photochemistry of polypyridine and porphyrin complexes* (Academic Press, 1992), chap. Photophysical properties of excited states, pp. 9–32.

[58] D. J. Nesbitt and R. W. Field, J. Phys. Chem. **100**, 12735 (1996).

[59] R. M. Stratt and M. Maroncelli, J. Phys. Chem. **100**, 12981 (1996).

[60] G. W. Flynn, C. S. Parmenter, and A. M. Wodtke, J. Phys. Chem. **100**, 12817 (1996).

[61] P. Hamm, S. M. Ohline, and W. Zinth, J. Chem. Phys. **106**, 519 (1997).

[62] A. Charvat, J. Abmann, B. Abel, D. Schwarzer, K. Henning, K. Luther, and J. Troe, Phys. Chem. Chem. Phys. **3**, 2230 (2001).

[63] E. M. S. Macoas, P. Myllyperkiö, H. Kunttu, and M. Pettersson, J. Phys. Chem. A, Submitted (2008).

[64] C. V. Shank, E. P. Ippen, and O. Teschke, Chem. Phys. Lett. **45**, 291 (1977).

[65] E. M. S. Macoas, R. Kananavicius, P. Myllyperkiö, M. Pettersson, and H. Kunttu, J. Am. Chem. Soc. **129**, 8934 (2007).

[66] J. P. Maier, A. Seilmeier, A. Loubereau, and W. Kaiser, Chem. Phys. Lett. **46**, 527 (1977).

[67] N. H. Damrauer, G. Cerullo, A. Yeh, T. R. Boussie, C. V. Shank, and J. K. McCusker, Science **275**, 54 (1997).

[68] G. Benkö, J. Kallioinen, J. E. I. Korppi-Tommola, A. Yartsev, and V. Sundström, J. Am. Chem. Soc. **124**, 489 (2002).

[69] L. S. Forster, Coord. Chem. Rev. **250**, 2023 (2006).

[70] A. C. Bhasikuttan and T. Okada, J. Phys. Chem. B **108**, 12629 (2004).

[71] K. F. Freed and J. Jortner, J. Chem. Phys. **52**, 6272 (1970).

[72] E. M. Kober, J. V. Caspar, R. S. Lumpkin, and T. J. Meyer, J. Phys. Chem. **90**, 3722 (1986).

[73] G. A. Voth and R. M. Hochstrasser, J. Phys. Chem. **100**, 13034 (1996).

[74] P. Chen and T. J. Meyer, Chem. Rev. **98**, 1439 (1999).

[75] E. M. S. Macoas, R. Kananavicius, P. Myllyperkiö, M. Pettersson, and H. Kunttu, J. Phys. Chem. **111**, 2054 (2007).

[76] J. Sykora and M. Hof, Cell. Mol. Biol. Lett. **7**, 259 (2002).

[77] K. Hashimoto, M. Hiramoto, and T. Sakata, J. Phys. Chem. **92**, 4272 (1988).

[78] T. Hamada, S. ichi Tanaka, H. Koga, Y. Sakai, and S. Sakaki, Dalton Trans. pp. 692–698 (2003).

[79] V. Lehtovuori, P. Myllyperkiö, J. Linnanto, C. Manzoni, D. Polli, G. Cerullo, M. Haukka, and J. Korppi-Tommola, J. Phys. Chem. B **109**, 17538 (2005).

[80] V. Lehtovuori, J. Aumanen, P. Myllyperkiö, M. Rini, E. T. J. Nibbering, and J. Korppi-Tommola, J. Phys. Chem. A **108**, 1644 (2004).

[81] V. Lehtovuori, J. Kallioinen, P. Myllyperkiö, M. Haukka, and J. Korppi-Tommola, Chem. Phys. **295**, 81 (2003).

[82] A. K. Holm, O. F. Mohammed, M. Rini, E. Mukhtar, and E. T. J. Nibbering, J. Chem. Phys. A **109**, 8962 (2005).

[83] L. X. Chen, G. B. Shaw, I. Novozhilova, T. Liu, G. Jennings, K. Attenkofer, G. J. Meyer, and P. Coppens, J. Am. Chem. Soc. **125**, 7022 (2003).

[84] G. B. Shaw, C. D. Grant, H. Shirota, E. W. C. Jr., G. J. Meyer, P. Coppens, and L. X. Chen, J. Am. Chem. Soc. **129**, 2147 (2007).

[85] R. A. Marcus and N. Sutin, Biochim Biophys Acta **811**, 265 (1985).

[86] R. A. Marcus, Annu. Rev. Phys. Chem. **15**, 155 (1964).

[87] R. A. Marcus, J. Chem. Phys. **24**, 966 (1956).

[88] R. A. Marcus, J. Chem. Phys. **43**, 679 (1965).

[89] R. J. D. Miller, G. L. McLendon, A. J. Nozik, W. Schmickler, and F. Willig, *Surface electron transfer processes* (VCH Publishers, Inc., 1995), chap. Theory of electrochemical electron transfer reactions, pp. 51–93.

[90] R. J. D. Miller, G. L. McLendon, A. J. Nozik, W. Schmickler, and F. Willig, *Surface electron transfer processes* (VCH Publishers, Inc., 1995), chap. Electron transfer at metal and semiconductor surfaces, pp. 95–166.

[91] T. Sakata, K. Hashimoto, and M. Hiramoto, J. Phys. Chem. **94**, 3040 (1990).

[92] J. Kallioinen, V. Lehtovuori, P. Myllyperkiö, and J. E. I. Korppi-Tommola, Chem. Phys. Lett. **340**, 217 (2001).

[93] J. Kallioinen, G. Benkö, V. Sundström, J. E. I. Korppi-Tommola, and A. P. Yartsev, J. Phys. Chem. **106**, 4396 (2002).

[94] M. O. Lenz and J. Wachtveitl, J. Phys. Chem. C **112**, 11973 (2008).

[95] R. Huber, J.-E. Moser, M. Grätzel, and J. Wachtveitl, Chem. Phys. **285**, 39 (2002).

[96] Y. Tachibana, J. E. Moser, M. Grätzel, D. R. Klug, and J. R. Durrant, J. Phys. Chem. **100**, 20056 (1996).

[97] J. B. Asbury, Y. Wang, and T. Lian, J. Phys. Chem. B **103**, 6643 (1999).

[98] D. Kuciauskas, J. E. Monat, R. Villahermosa, H. B. Gray, N. S. Lewis, and J. K. McCusker, J. Phys. Chem. B **106**, 9347 (2002).

[99] B. Wenger, M. Grätzel, and J.-E. Moser, J. Am. Chem. Soc. **127**, 12150 (2005).

[100] J. B. Asbury, R. J. Ellingson, H. N. Ghosh, S. Ferrere, A. J. Nozik, and T. Lian, J. Phys. Chem. B **103**, 3110 (1999).

[101] M. J. Weaver, G. E. McManis, W. Jarzeba, and P. F. Barbara, J. Phys. Chem. **94**, 1715 (1990).

[102] P. F. Barbara, T. J. Meyer, and M. A. Ratner, J. Phys. Chem. **100**, 13148 (1996).

[103] J. M. Rehm, G. L. McLendon, Y. Nagasawa, J. Moser, and M. Grätzel, J. Phys. Chem. **100**, 9577 (1996).

[104] P. Hamm, R. A. Kaidl, and J. Stenger, Opt. Lett. **25**, 1798 (2000).

[105] S. Das and P. Kamat, J. Phys. Chem. **102**, 8954 (1998).

[106] G. Boschloo and A. Hagfeldt, Chem. Phys. Lett. **370**, 381 (2003).

[107] G. Benkö, M. Hilgendorff, A. P. Yartsev, and V. Sundström, J. Phys. Chem. B **105**, 967 (2001).

[108] T. Kitamura, M. Ikeda, K. Shigaki, T. Inoue, N. A. Anderson, X. Ai, T. Lian, and S. Yanagida, Chem. Mater **16**, 1806 (2004).

[109] R. J. Ellingson, J. B. Asbury, S. Ferrere, H. N. Ghosh, J. R. Sprague, T. Lian, and A. J. Nozik, J. Phys. Chem. B **102**, 6455 (1998).

[110] K. B. Eisenthal, Acc. Chem. Res. **6**, 118 (1975).

[111] G. R. Fleming, *Chemical applications of ultrafast spectroscopy* (Oxford University Press, 1986), chap. Relaxation processes in liquids and solutions, pp. 124–235.

[112] D. P. Millar, R. Shah, and A. H. Zewail, Chem. Phys. Lett. **66**, 435 (1979).

[113] H. E. Lessing and A. V. Jena, Chem. Phys. Lett. **42**, 213 (1976).

[114] O. Svelto, *Principles of lasers 3rd ed.* (Plenum Press, New York, 1989), chap. Laser beam transformation: Propagation, amplification, frequency conversion, pulse compression, pp. 411–453.

[115] C. Rullière, ed., *Femtosecond Laser Pulses: Principles and experiments 2nd Ed.* (Springer, 2003), chap. Pulsed optics, pp. 25–56.

[116] C. Rullière, ed., *Femtosecond Laser Pulses: Principles and experiments 2nd Ed.* (Springer, 2003), chap. How to manipulate and change the characteristics of laser pulses, pp. 187–193.

[117] *Snlo non-linear optics code available from a. v. smith, as-photonics, albuquerque, nm.*

[118] E. Riedle, M. Beutter, S. Lochbrunner, J. Piel, S. Schenkl, S. Spöderlein, and W. Zinth, Appl. Phys. B. **71**, 457 (2000).

[119] L. C. Ltd., *Biophysical techniques in photosynthesis* (Kluwer Academic Publishers, 1996), chap. Operation principles, pp. 75–92.

[120] J. Amesz and A. J. Hoff, eds., *Biophysical techniques in photosynthesis* (Kluwer Academic Publishers, 1996), chap. Data analysis of time-resolved measurements, pp. 75 92.

[121] I. H. M. Stokkum, D. S. Larsen, and R. van Grondelle, Biochimica et biophysica acta **1657**, 82 (2004).

[122] M. K. Nazeeruddin, A. Kay, I. Rodicio, R. Humbry-Baker, E. Mûller, P. Liska, N. Vlachopoulos, and M. Grätzel, J. Am. Chem. Soc. **115**, 6382 (1993).

[123] M. Grätzel, Nature **414**, 338 (2001).

[124] S. Fantacci, F. D. Angelis, and A. Selloni, J. Am. Chem. Soc. **125**, 4381 (2003).

[125] F. D. Angelis, S. Fantacci, and A. Selloni, Chem. Phys. Lett. **389**, 204 (2004).

[126] H. Rensmo, S. Södergren, L. Patthey, K. Westermark, L. Vayssieres, O. Kohle, P. A. Bruhwiler, A. Hagfeldt, and H. Siegbahn, Chem. Phys. Lett. **274**, 51 (1997).

[127] H. Rensmo, S. Lunell, and H. Siegbahn, J. Photochem. Photobiol. A **114**, 117 (1998).

[128] E. M. J. Johansson, M. Hedlund, H. Siegbahn, and H. Rensmo, J. Phys. Chem. B **109**, 22256 (2005).

[129] P. Persson and M. J. Lundqvist, J. Phys. Chem. **109**, 11918 (2005).

[130] J.-F. Guillemoles, V. Barone, L. Joubert, and C. Adamo, J. Phys. Chem. A **106**, 11354 (2002).

[131] M. Nazeeruddin, S. Zakeeruddin, R. Humbhry-Baker, M. Jirousek, P. Liska, N. Vlachopoulos, V. Shklover, C.-H. Fischer, M. G. Kay, I. Rodicio, et al., Inorg. Chem. **38**, 6298 (1999).

[132] M. R. Waterland and D. F. Kelley, J. Phys. Chem. A **105**, 4019 (2001).

[133] J. B. Asbury, E. Hao, Y. Wang, H. N. Ghosh, and T. Lian, J. Phys. Chem. A **105**, 4545 (2001).

[134] S. Wallin, J. Davidsson, J. Modin, and L. Hammarström, J. Phys. Chem. A **109**, 4697 (2005).

[135] T. Hannappel, B. Burfeindt, W. Storck, and F. Willig, J. Phys. Chem. B **101**, 6799 (1997).

[136] T. A. Heimer, E. J. Heilweil, C. A. Bignozzi, and G. J. Meyer, J. Phys. Chem. A **104**, 4256 (2000).

[137] C. Bauer, G. Boschloo, E. Mukhtar, and A. Hagfeldt, J. Phys. Chem. B **105**, 5585 (2001).

[138] J. Kallioinen, G. Benkö, P. Myllyperkiö, L. Khriachtchev, B. Skårman, R. Wallenberg, M. Tuomikoski, J. Korppi-Tommola, V. Sundström, and A. Yartsev, J. Phys. Chem. B **108**, 6365 (2004).

[139] B. I. Lemon and J. T. Hupp, J. Phys. Chem. B **101**, 2426 (1997).

[140] Y. Tachibana, M. Nazeeruddin, M. Grätzel, D. R. Klug, and J. R. Durrant, Chem. Phys. **285**, 127 (2002).

PAPER I

Reproduced with permission from
"Transient absorption studies of the $Ru(dcbpy)_2(NCS)_2$ excited state and the dye cation on nano-crystalline TiO_2 film", Kallioinen, J.; Lehtovuori, V.; Myllyperkiö, P.; Korppi-Tommola, J.E.I., *Chemical Physics Letters* **2001**, 340, 217-221.

https://doi.org/10.1016/S0009-2614(01)00398-0

PAPER II

Reproduced with permission from
"Photoinduced Electron Injection from $Ru(dcbpy)_2(NCS)_2$ to SnO_2 and TiO_2 Nanocrystalline Films", Benkö, G.; Myllyperkiö, P.; Pan, J.; Yartsev, A.P.; Sundström, V., *Journal of American Chemical Society* **2003**, 125, 1118-1119.

https://doi.org/10.1021/ja029025j

PAPER III

Reproduced with permission from
"Interligand Electron Transfer Determines Triplet Excited State Electron Injection in RuN3-Sensitized TiO_2 Films", Benkö, G.; Kallioinen, J.; Myllyperkiö, P.; Trif, F.; Korppi-Tommola, J.E.I.; Yartsev, A.P.; Sundström, V., *Journal of Physical Chemistry B* **2004**, 108, 2862-2867.

https://doi.org/10.1021/jp036778z

PAPER IV

Reproduced with permission from
"A study of electron transfer in $Ru(dcbpy)_2(NCS)_2$ sensitized nanocrystalline TiO_2 and SnO_2 films induced by red-wing excitation", Myllyperkiö, P.; Benkö, G.; Korppi-Tommola, J.; Yartsev, A.P.; Sundström, V., *Physical Chemistry Chemical Physics* **2008**, 10, 996-1002.

https://doi.org/10.1039/B713515G

PAPER V

Reproduced with permission from
"Photoinduced interfacial electron injection in RuN3-TiO_2 thin films: Resolving picosecond timescale injection from the triplet state of the protonated and deprotonated dyes", Pellnor, M.; Myllyperkiö, P.; Korppi-Tommola, J.; Yartsev, A.; Sundström, V., *Chemical Physics Letters* **2008**, 462, 205-208.

https://doi.org/10.1016/j.cplett.2008.07.066

PAPER VI

A manuscript of
"Electron Transfer from Organic Aminophenyl Acid Sensitizers to Titanium Dioxide and Aluminum Oxide Nanoparticle Films", Myllyperkiö, P.; Manzoni, C.; Polli, D.; Cerullo, G.; Korppi-Tommola, J., Submitted to the *Journal of Physical Chemistry C* **2008.** Unpublished work.

https://doi.org/10.1021/jp902226y

PAPER VII

Reproduced with permission from
"Ultrafast Electronic and Vibrational Energy Relaxation of Fe(acetylacetonate)$_3$ in Solution", Macoas, EM.S.; Kananavicius, R.; Myllyperkiö, P.; Pettersson, M.; Kunttu, H., *Journal of Physical Chemistry A* **2007**, 111, 2054-2061.

https://doi.org/10.1021/jp066271z